Exploiting the Interactions of Solid Binding Proteins with Silica to form Colloidal Assemblies

Julia Boese

A thesis

submitted in partial fulfillment of the

requirements for the degree of

Master of Science in Chemical Engineering

University of Washington

2020

Committee:

François Baneyx

Jim Pfaendtner

Program Authorized to Offer Degree:

Department of Chemical Engineering

University of Washington

Abstract

Exploiting the Interactions of Solid Binding Proteins with Silica to form Colloidal Assemblies

Julia Boese

Chair of the Supervisory Committee:

François Baneyx

Department of Chemical Engineering

Solid binding peptides (SBPs) are short sequences of amino acids selected by combinatorial techniques for their high affinity for inorganic surfaces. When genetically encoded within proteins, SBPs can function as linkers to create hybrid materials comprising inorganic components and the proteins to which they are fused. Here, we show how such solid binding proteins may be employed to achieve dynamic control over the assembly and disassembly of silica nanoparticles and how the process is influenced by SBP sequence, insertion point within the protein, and solution conditions. Using fluorescent-resonant energy transfer (FRET), dynamic light scattering (DLS) and scanning electron microscopy (SEM), we show that bifunctional derivatives of superfolder green fluorescent protein (sfGFP) engineered with two strong, or with a strong and a weak silica-binding peptide support the pH-dependent aggregation and disaggregation of rhodamine-containing silica nanoparticle (RhSiNP). We further demonstrate that pH shifts can be used to cycle nanoparticles between assembled and dispersed states and that aggregate size can be tuned with different SBPs, NP sizes, and salt concentrations.

Additionally, we designed multimeric *de novo* and natural proteins for increased control over the pattering of silica nanoparticles (SiNPs) and designed ZnS binding and cysteine binding sfGFP for the association of QDs into protein-linked nanomaterials. This new paradigm for the synthesis of dynamic nanoparticle systems should find applications in biosensing, diagnostics, and advanced materials.

Table of Contents

List of Figures

List of Tables

Acknowledgements

There are plenty of people I would like to thank for supporting me over the last two years: My advisor, François Baneyx, for guiding me during my work, my lab-mates for their camaraderie and our lunches and coffee runs, my additional mentors Allison and Cole and my friends and colleagues in the department and CSSAS for giving me great ideas and bolstering my spirits during our social activities and happy hours. I also want to thank my family for their love and support even when they did not quite understand what I was doing or why. Most of all, I would like to thank my friends Ashley and Weston for supporting me though the most difficult of times and every bump in the road, and together along with Percy and Toothless, you were able to make me smile and relax.

Chapter 1 Introduction

Nanomaterials have long been known to possess unique mechanical, colloidal, electronic and various other properties that allow for the design of novel engineering systems and sensors.[1–3] For example, the electrons of quantum dots are confined to specific energy levels based on the size of the dot, lending to unique applications as biological markers or as semiconductors.[4] Despite promising advances in science and technology at the nanoscale, ordered assembly and dynamic control over these materials remains difficult and inefficient[2,3] The traditional approach to nanomaterial assembly is through 'top down' techniques such as lithography, milling, or electrospinning which are normally less expensive and/or easier to control than 'bottom up' techniques like chemical vapor deposition (CVD) or electrodeposition.[5]

More recently, nanofabrication research has trended toward self-assembly; focusing on how nature solves challenges in energy storage, transportation, and structuring, on the nano to mesoscale.[6,7] Organisms resolve these challenges through self-assembly of biomacromolecules such as proteins and peptides which act as building blocks and scaffolds for larger, more complex architectures.[8,9] These proteins and biomolecules fabricate materials with nanoscale precision and understanding how to control protein-guided materials synthesis would open up a range of applications in biosensing, drug delivery, and protein-templated device fabrication.[9]

This work focuses on: (1) using homobifunctional silica-binding proteins to design hybrid architectures, (2) developing predictive dynamic control over the properties of these architectures, and (3) on expanding our knowledge of solid binding proteins to apply to multi-valent proteins and different molecular inorganic building blocks such as quantum dots and magic-sized clusters. We ask these questions within the context of the solid-binding peptide Car9, a solid binding peptide (SBP) chosen for our understanding of its ability to interact with silica and more explicitly our

understanding of the effect of its insertion location within a scaffold, oligomerizing capabilities, and binding model. The goal of this work is to further understand and exploit the interactions between Car9-tagged proteins and silica surfaces, specifically, in terms of dynamically controlling colloidal assembly of SiNP bridged by Car9-tagged proteins. More specifically, we study how Car9 and its variants allow for dynamic control over the assembly of hybrid materials at different solution conditions. Our long-term goals include predictively assembling complex and organized hybrid architectures with dynamic control and to expand our ability to use cysteine chemistry and other solid binding peptides to assemble further hybrid architectures.

1.1 Hybrid and Nanomaterial Assembly

Hybrid materials are those that incorporate both organic and inorganic components[10], while nanomaterials consist of nanoparticles that range in size between 1-100nm[11] although neither are well-defined across the discipline. Both types of materials have emergent properties (**Figure 1.1**) derived from either their integration of organics and inorganics or the capability of nanoparticle

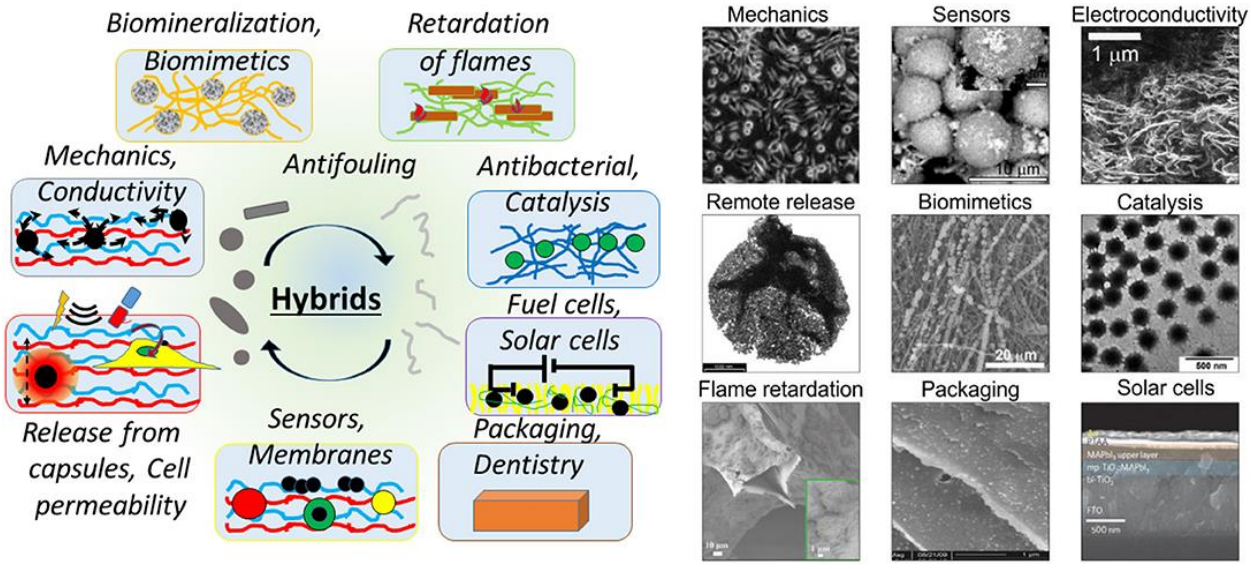

Figure 1.1 Various applications of hybrid materials.[10]

properties differing from the bulk, leading to increasing interest in developing both of these materials.[10,11] Commonly used approaches of assembly for hybrid and nanomaterials include

spontaneous colloidal crystallization, guided assembly on patterned substrates,[12,13] assembly in emulsions, and light or magnetic field driven assembly.[14–16] Additionally, connecting particles with nucleic acids, polymers, ligands, and peptides have been explored.[6,17–20]

Grafting DNA to gold NPs allows for a temperature-based control of NP aggregation where the dissociation stimuli is dependent on the melting of DNA bridges between bound particles.[20] Further use of DNA-bound gold NPs or clusters shows that they can be assembled into soluble aggregates that are discrete, well-defined and, homogeneous[21] or nanocrystals with various lattice structures, symmetry, or size.[18,19,22] Although DNA-NP systems have been developed with light and temperature based dynamic control and reversibility[23], large-scale fabrication of these materials remains costly and inefficient for practical use. Polymers and ligands conjugated to NPs have also been used to create nanomaterials and thin films with varying degrees of control and reversibility.[24–28] These materials often aggregate due to hydrogen bonding between polymers/ligands and can be reversibly controlled to some extent by altering surface deprotonation through large pH shifts around their pKa although due to the conjugation of these ligands and polymers to the surface this can cause NP destabilization.[25,29,30] Nevertheless, conducting particle assembly with these methods can be limited by the number of available interactions and the length scales.[31,32]

Proteins and peptides often play a key role in biomineralization and bio-aggregation processes and are responsible for transporting, storing, precipitating and templating inorganic components into ordered and often dynamic assemblies.[3,33] Organized from the nano to the mesoscale, hybrid materials containing organic and inorganic components can have a finely tuned hierarchical structures self-assembled and determined by protein or peptide building blocks.[6,7] Although protein or peptide-coated NP are often used to induce increased bioactivity or biocompatibility,[34–

[36] proteins and various peptides can also be used to synthesize nanomaterials.[37–39] Protein coronas often form around NP *in vivo* and research shows that the addition of a protein, typically lysozyme, can cause aggregation of NPs upon protein absorption and unfolding.[37,38] Furthermore, some control over the aggregation and NP density can be controlled over large pH ranges between the isoelectric points of the building blocks.[39] Additionally, peptide-NP conjugates, specifically featuring solid-binding peptides, have been used to create various types of nanomaterials through self-assembly, though often these materials lack dynamic control.[40]

1.2 Solid Binding Peptides and Car9, a Silica-Binding Peptide

For decades, solid binding peptides (SBPs) have been used to study biotic-abiotic interactions and to organize organic and inorganic components for nanobiotechnology applications. SBPs are short stretches of amino acids, typically 7 to 12 residues long that are isolated by phage or cell surface display.[3,8] They generally exhibit high selectivity and affinity to surfaces of inorganic or organic materials and can be genetically fused to, or inserted within, larger protein frameworks to endow an SBP with higher stability and solubility.[8] Furthermore, insertion of multiple SBPs within a single protein framework provides an ability to bind or mineralize several inorganic components, and to build complex architectures that have been used in biomaterial production, nanostructure fabrication, and biomedical applications. Within this context we use solid binding proteins to drive the assembly of nanoparticles to access a much larger chemical and structural design space than seen with DNA assemblies.

The Car9 (DSARGFKKPGKR) SBP was originally identified to bind with carbonaceous substrates, exhibiting a preference for sp^3-hybridized carbon,[41] and was shown to exhibit high affinity for the negatively charged silanol (Si-OH) groups of silica (SiO_2).[42,43] The promiscuous binding profile and ability for the Car9-silica interactions to be disrupted by the addition of lysine

or arginine has enabled various applications including affinity protein purification, microcontact printing, controlled protein release, and hybrid materials assembly.[35,43–47] Using surface plasmon resonance (SPR), we found that Car9-tagged proteins exhibit sigmoidal adsorption sensorgrams on silica surfaces and to account for this behavior we developed a two-step model capturing the cooperative interactions and adsorption kinetics of Car9-tagged proteins.[48] Furthermore, Rosetta and MD simulation suggest that Car9's lysine (K) residues form a tripod-like structure projecting from a central core along with equatorial arginine (R) residues.[49] These basic residues play an essential role in promoting interactions between Car9 and silica surfaces and when two of the basic residues in the Car9 peptide involved in silica binding are mutated to neutral alanines, it becomes possible to model adsorption kinetics with a classic Langmuir fit.[49] With these mutations, Car9(K8AK11A) also loses some of its ability to oligomerize on silica surfaces forming single structures and dimers more often when compared to the trimers and tetramers formed with WT Car9-tagged sfGFP.[49]

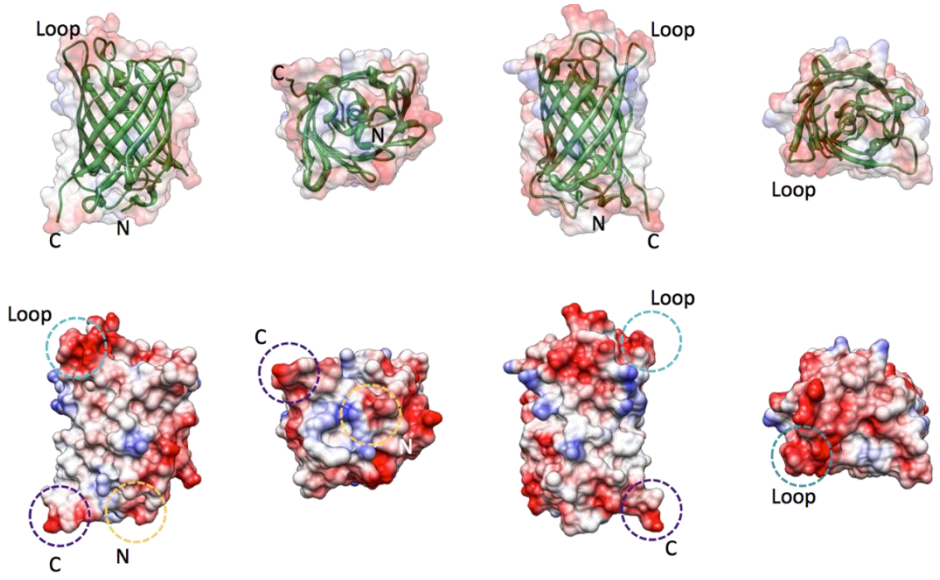

Figure 1.2 Ribbon representation (top) of the sfGFP framework showing the locations of loop 9 (Loop) and of the amino- (N) and carboxy- (C) termini in front, bottom, back and top orientations. Electrostatics are rendered on the molecular surface (bottom panel) between -10kTe (red) and +10kTe (blue).

We have used monovalent derivatives of sfGFP with a single Car9 silica-binding peptide genetically installed at the C-terminus (sfGFP-Car9) or within permissive loop 9 (sfGFP::Car9) (**Figure 1.2**) to determine how the local structure and electrostatics of the insertion point would influence materials-binding properties. We used SPR to probe binding kinetics on silica-coated chips and conducted the experiment under two conditions of pH (7.5 and 8.5) to determine how deprotonation of surface silanols (≡SiOH) would influence binding.[50–52] We found that protein surface coverage, was greater for sfGFP-Car9 compared to sfGFP::Car9 at pH 7.5 and with an increase of pH to 8.5, surface coverage decreased about 30%.[53]

1.3 Chemistry and Peptide/Protein Absorption of Silica Nanoparticles

Silica in bulk and as a nanoparticle is a material that has been used in catalysis, separation processes, biomedical functions, and pharmaceuticals due to its biocompatibility, binding capability, stability, and abundance.[54,55] Colloidal silica has also been widely used as a surfactant and to improve rheological properties of cosmetics and transdermal applications.[56] Colloidal silica particles interact through Van der Waals attraction and electric double layer repulsions forces, as described by Derjaguin, Landau, Verwey, and Overbeek (DLVO) theory.[4,57]

The surface of silica particles is negatively charged at neutral pH and is dependent of the deprotonation of silanol groups at the surface which can exist as isolated silanols (≡Si−OH), geminal silanols (=Si(OH)$_2$), or vicinal silanols (H-bonded silanols) depending on the crystal structure and synthesis method. [58] At acidic pH between pH 2-4, silica surfaces are neutral, and become more and more negative with increasing pH, as is consistent with the Stern model.[59] As per double layer theory, the addition of ions or salt, shrink double layers surrounding nanoparticles, leading to increased aggregation at increased salt concentrations.[57,59] The valency of the

counterions, the concentration of the nanoparticles, and the surface chemistry of the nanoparticles all affect the ability of these systems to aggregate and the rate at which aggregation occurs.[57]

While the understanding of protein absorption on flat surfaces is bolstered by years of experimentation, a significant gap remains in our understanding of protein absorption on curved surfaces like nanoparticles.[60] Previous studies show that adsorption of specific silica-binding peptides on nanoparticles is driven by various interactions including electrostatics, hydrophobic interactions, hydrogen bonding, ion-ion, ion-dipole, and Van der Waals interactions between the nanoparticles and the surface.[51,61] Continuing, both an increase in particle size and pH resulted in increased surface ionization leading to increased concentrations of the bound peptide.[51] It is this knowledge of how pH, salt concentration, nanoparticle size and DLVO theory that drives our investigation.

1.4 Förster Resonance Energy Transfer

One way to measure distance between molecular particles is to use Förster resonance energy transfer (FRET). FRET occurs when two chromophores with overlapping spectra are in close enough proximity that the emission of the donor chromophore is able to excite the chromophore of the acceptor.[62] Molecules can only generate FRET signal if all off of the following conditions are met; 1) the emission spectrum of the donor must overlap with the absorption spectrum of the acceptor molecule, 2) the distance between chromophores must be less than 10nm, and 3) there must be long-range interactions between the donor and acceptor molecules.[62] There are various ways to measure the FRET efficiency of a pair of molecules, although most commonly, the efficiency is determined by measuring the change in donor fluorescence intensity when an acceptor molecule is added to the system.[63] Like most systems based on light scattering or fluorescence, the FRET efficiency is inversely proportional to the distance between donor and acceptor molecules

raised to the sixth power. The Förster radius (R_0) corresponds to the distance at which energy transfer between two particular chromophores is 50% efficient and it can be calculated in Å by:

$$R_0 = [8.8 \times 10^{23} . \kappa^2 . n^{-4} . QY_D . J(\lambda)]^{1/6} \quad \text{(I)}$$

Where κ^2 is the dipole orientation factor, taken as 2/3 for randomly oriented donors and acceptors, QY_D is the quantum yield of sfGFP in the absence of Rhodamine B which is equal to 0.65, *n* is the refractive index of the buffer which is equal to 1.33 and $J(\lambda)$ is the spectral overlap integral in cm^3M^{-1}.[64] With one-to-one donor to acceptor systems, one can use FRET efficiency to calculate the characteristic distance between chromophores (*R*) by the equation:

$$R = R_0 \sqrt[6]{\frac{1-E}{E}} \quad \text{(II)}$$

Where E is the calculated FRET efficiency.

FRET has been commonly used as a molecular ruler for distances between particular fluorescent molecules, helping evolve fields of biological research such as membrane mapping and protein interaction studies.[63,65,66] Organic dyes such as Rhodamine, inorganic ions like Yb^{3+}, fluorescent proteins like GFP, CFP, or YFP, and quantum dots are often used in FRET pairs. [63] While the model system is between CFP-YFP pairs, many other FRET pairs are possible.[63] For systems with multiple donors and acceptors, interactions become complicated, lending to the FRET measurements not being accurate for precise distance calculations. Specifically, increasing numbers of donors and acceptors do not change the FRET efficiency in a proportional way, relationships between the efficiency and the distance become non-proportional.[65,66]

Chapter 2 Chemical Control of Colloidal Assembly with Homobifunctional Solid-Binding Proteins

2.1 Introduction

Previously, we reported on the use of the C-terminus and loop 9 of sfGFP (a permissive location that tolerates the insertion of extraneous amino acids)[67] to display SBPs with distinct materials specificity on opposite sides of the GFP β-barrel. We used these heterobifunctional solid-binding proteins to mineralize manganese-doped zinc sulfide nanocrystals and couple them to silica,[35] and to decorate carbon nanotubes with gold nanoparticles.[44] However, we did not fully explore the use of homobifunctional derivatives of sfGFP that incorporate the same SBP on either side of the β-barrel to create supramolecular structures, and we did not consider the manipulation of solution conditions and SBP sequence as a means to control assembly outcomes. Preliminary studies showed that using the homo-bifunctional dual-tagged sfGFP::Car9-Car9 could assemble RhSiNP at pH 7.5 at an average size of 1700nm while the mutated sfGFP::Car9-K8AK11A produced smaller assemblies at 520nm. At pH 8.5 both assemblies of protein and NP disassembled into single protein-bound nanoparticles and cycling between pH 7.5 and pH 8.5 produced a cycle of assembly and disassembly of the structures (**Figure 2.1**).

Here, we combine SPR measurements, dynamic light scattering (DLS), and Förster resonance energy transfer (FRET) to explore the solution conditions in which assembly and disassembly of RhSiNP-protein aggregates can be controlled. Additionally, we explore how various NP size, and protein ratio will affect the aggregation behavior of this system through the use of varying RhSiNP sizes and expanding the system to SiNP.

2.2 Materials and Methods

2.2.1 DNA manipulations and protein purification. Plasmid pET24a(+)- sfGFP encodes a derivative of superfolder green fluorescent protein (sfGFP) modified.[43] Plasmid pET24a(+)-

sfGFP::Car9 encodes sfGFP::Car9, containing the Car9 sequence within a permissive loop inserted between *BamHI* and *SpeI* digestive sites. Plasmid pET24a(+)-sfGFP::Car9-Car9 encodes sfGFP::Car9-Car9, a derivative of sfGFP-Car9 with an additional Car9 tag introduced within the same permissive loop as sfGFP::Car9, inserted between *BamHI* and *SpeI* digestive sites. Plasmid pET24a(+)-sfGFP::Car9-K8AK11A encodes sfGFP::Car9-K8AK11A, a derivative of sfGFP::Car9-Car9 containing the Lys-8 to Ala and Lys-11 to Ala substitutions in the C-terminal Car9 sequence. The integrity of all constructs was verified by DNA sequencing and plasmids were introduced into *E. coli* BL21(DE3).

Car9-expressing cultures were grown and induced, and proteins purified by silica affinity purification as described.[43,46] Wild type sfGFP was purified from BL21(DE3) cells harboring pET24a(+)-sfGFP by Fast Protein Liquid Chromotagraphy (FPLC) using a BioRad DEAE ion exchange chromatography column. The protein was loaded onto the column and washed using Tris-HCl, pH 7.5 and eluted using a gradient elution with 20mM Tris-HCl, 1M NaCl, pH 7.5. Protein were concentrated to about 50mg/mL in 20mM Tris-HCl, pH 7.5 using an Amplicon microconcentrator, aliquoted, and stored at -20C.

2.2.2 pH cycling for protein-NP solutions. The rhodamine-conjugated silica nanoparticles (RhSiNP) or silica nanoparticles (SiNP) terminated with surface silanols and 10nm or 30nm in diameter and concentrated to 25 mg/mL were purchased from Micromod Partikeltechnologie GmbH (Rostock, Germany). To assess the effect of pH on protein-mediated assembly or disassembly of 10nm RhSiNP or SiNP, protein and nanoparticle were mixed to a final concentration of 5μM protein and 1μM RhSiNP in 20mM Tris-HCl, pH 7.5. For the 30nm RhSiNP a final concentration of 9μM protein to 0.2 μM RhSiNP is used. The final volume of the mixed solution was between 500μL and 3mL and were stored in either a 2mL Eppendorf tube or a 15mL

capped-conical tube. The protein-NP solutions were then mixed on a tube rotator for 30 minutes before acquisition of, FRET, DLS, ζ-potenital, or SEM measurements. For pH cycling experiments, samples were prepared and data collected as stated above. Samples were then treated with 1M NaOH added in 1 μL increments and after each addition the tube was inverted 4-6 times prior to pH measurement with a Mettler Toledo microtip pH electrode. Once the solution reached pH 8.5, the tube was placed on a tube rotator for 30 minutes before data acquisition. To acidify the solution back to pH7.5, 1M HCl was added in the same quantity used to alkalize the solution and then the tube was placed on a tube rotator for 30 minutes prior to data acquisition. Throughout acidification and alkalization process an average of 5mM Na^+ or 5mM Cl^- is added per cycle while a maximum of 10mM Na^+ or 10mM Cl^- is added to the solution per cycle.

2.2.3 Analytical Techniques. Surface plasmon resonance (SPR) experiments were conducted using ethanol and UV-ozone treated silica-coated SPR chips fabricated in house[41] and mounted on the flow cell of a SPR sensor from the Institute of Photonics and Electronics (Prague, Czech Republic). Experiments were conducted at a protein concentration of 0.1-0.2 μM, a flow rate of 50 $\mu L min^{-1}$ and a temperature of 25°C. Förster Resonance Energy Transfer (FRET) measurements were acquired on a 500μL sample in a 10 cm path length quartz cuvette using a F4500 fluorescence spectrophotometer (Hitachi) with an excitation wavelength of 485 nm (sfGFP), slit widths at 2.5 nm and a scan speed of 240 nm/min. FRET efficiency was calculated by measuring the change in the donor fluorescence intensity in the absence and presence of acceptor, using:

$$E = 1 - \frac{I_{DA}}{I_D} \quad \text{(I)}$$

where I_{DA} and I_D are the total donor fluorescence intensities in presence and absence of acceptor respectively.[63] A Zetasizer Nano ZS (Malvern Instruments) was used to monitor NP and protein sizes and the formation of aggregates. Measurements comprising 12-20 measurement cycles were

performed on 500μL of samples prepared in three independent experiments. Zeta potentials were measured on the same instrument using folded capillary cells (DTS1070, Malvern Instruments). Statistical analysis was completed using a Student's t-test.

2.3 Results and Discussion

2.3.1 Influence of framework insertion point and solution pH on the silica binding affinity of the Car9 SBP. In previous work we used monovalent derivatives of sfGFP with a single Car9 silica-binding peptide genetically installed at the C-terminus (sfGFP-Car9) or within permissive loop 9 (sfGFP::Car9) to determine how the local structure and electrostatics of the insertion point would influence materials-binding properties (**Fig, A.1**).[53] We used SPR to probe binding kinetics on silica-coated chips and conducted the experiment under two conditions of pH (7.5 and 8.5) to determine how deprotonation of surface silanols (≡SiOH) would influence binding.[50–52] To supplement these SPR studies, we exploited the biological fluorescence of the sfGFP framework and the commercial availability of silica nanoparticles encapsulating rhodamine dye (hereafter referred to as RhSiNP) to develop a fluorescence resonance energy transfer (FRET) assay in which sfGFP serves as the donor and RhSiNP serves as the acceptor (**Fig. A.2A**). While the overlap between the sfGFP emission band and the rhodamine absorption spectrum is only partial (**Fig. A.2B**), there is no cross-talk between the two chromophores (**Fig. A.2C**), and neither the emission of the donor (**Fig. A.2D**) nor that of the acceptor (**Fig. A.2E**) is affected in the pH 7.5 to 8.5 range. This technique was used in previous studies, but my work elucidated that the RhSiNP used caused no differences from the assumptions made based on Rhodamine B dye and that the pH was not affecting the spectra of either the sfGFP and the RhSiNP.

Having previously shown that insertion of SBPs within loop 9 and at the C-terminus of sfGFP does not affect the spectral characteristics of the protein,[29] we used dynamic light scattering

(DLS, **Fig. A.3A**) to determine the hydrodynamic diameter of RhSiNP nanoparticles (17.6 ± 1.2 nm at pH 7.5 and 17.1 ± 1.3 nm at pH 8.5 which is consistent with the manufacturer's specified size of 10 nm). We also use zeta potential measurements to confirm the manufacturer's assertion that rhodamine is encapsulated within a silica matrix and that the surface of the nanoparticles has similar Zeta potentials to those terminated by silanol and silane groups. Zeta potential values were -24.7 ± 0.5 mV at pH 7.5 which is consistent with the -20 mV to -30 mV range previously reported for silica nanoparticles of similar sizes at neutral pH.[51,68,69] At pH 8.5, the zeta potential increased to and -34.9 ± 9.9 mV, likely reflecting deprotonation of silanol groups and an increasing amount of surface siloxides ($\equiv SiO^{-\cdots}Na^{+}$). This value is consistent with the results of Puddu and Perry who supported that zeta potential values decrease with increasing pH.[61]

We previously used FRET to show that energy transfer was about 60% higher between sfGFP::Car9 and RhSiNP compared to sfGFP-Car9, a result that is well explained by the fact that a loop-displayed Car9 should bring the sfGFP chromophore in closer proximity to silica-encapsulated rhodamine molecules than a C-terminally fused Car9[53] (see **Fig. A.2A** for a schematic illustration). Consistent with SPR data, and as would be expected from less frequent interactions between donor and acceptor, increasing the pH by one unit led to an about 30% decrease in FRET efficiency (**Table 1**). Also, we have shown that the K8AK11A mutant

Table 1: FRET efficiencies between 10 nm RhSiNP and the indicated sfGFP variants (*Data collected by Yundi Zhao[53])

Protein	pH 7.5	pH 8.5	Percent Decrease
sfGFP*	0.034	0.031	8.8%
sfGFP::Car9*	0.147	0.102	30.6%
sfGFP-Car9*	0.092	0.065	29.3%
sfGFP-K8AK11A*	0.077	0.036	53.2%
sfGFP::Car9-Car9	0.286	0.111	61.2%
sfGFP::Car9-K8AK11A	0.227	0.111	51.1%

significantly reduced affinity for silica,[49] thus we were not surprised to observe a lower FRET efficiency for the sfGFP-K8AK11A variant relative to sfGFP-Car9 at pH 7.5 or the decrease in efficiency at pH 8.5.

2.3.2 Chemical control of colloidal assembly with homobifunctional solid-binding proteins. The availability of two pH-addressable insertional locations with different affinities for silica along with that of a low-affinity Car9 mutant provided us with an opportunity to explore protein-based control of RhSiNP assembly and disassembly. To this end, we constructed sfGFP::Car9-Car9, which contains Car9 insertions at both the C-terminus and within loop 9 of sfGFP, and sfGFP::Car9-K8AK11A in which the wild type Car9 C-terminal extension is exchanged for that of the K8AK11A mutant.

At pH 7.5, we observed a 2 to 3-fold increase in FRET efficiencies with both proteins (**Table 1**) which we attribute to contributions from multiple donors and acceptors caused by the bridging of RhSiNPs and the formation of clusters of protein-linked nanoparticles.[65,66] Consistent with the behavior of monovalent sfGFP-K8AK11A, and as evidenced by the lower FRET efficiency of the sfGFP::Car9-K8AK11A-RhSiNP system at pH 7.5, the mutant C-terminal extension appeared less effective than wild type Car9 at promoting such bridging interactions. Nevertheless, energy transfer efficiencies decreased to ~11% for both homobifunctional proteins preparations when the pH was adjusted to 8.5 (**Table 1**). This value is comparable to the FRET efficiency observed with monovalent sfGFP::Car9 and RhSiNP under alkaline conditions, suggesting that raising the solution pH by a single unit might be sufficient to weaken bridging interactions and promote aggregate dissociation.

To test these hypotheses, we performed DLS measurements of size distribution using a 5:1 molar ratio of protein to RhSiNP particles and 30 minutes of incubation. Control experiments

conducted with wild type sfGFP revealed no interactions between nanoparticles and the protein framework (**Fig. A.3A**). On the other hand, both sfGFP-Car9 and sfGFP::Car9 when mixed with the 10nm RhSiNPs shifted the mean D_h of RhSiNP from 17.6 ± 1.2 nm for naked nanoparticles to 21.3 ± 4.4 nm and 18.2 nm, respectively (**Fig. A.3B**). It is interesting to note that the sfGFP-Car9 and RhSiNP sample is polydisperse with a second peak at 380 ± 110 nm. Since larger particles scatter light proportionally to the sixth power,[70] there may not be many of these larger scattering centers even if a prominent peak is shown. This is supported because when the number percent is calculated instead of intensity reading to account for this power difference, this peak disappears. Otherwise, this can possibly be explained by the oligomerizing abilities of Car9 and hence sfGFP-Car9. Since we know that sfGFP-Car9 does not bind as closely to the nanoparticle surface, it is possible that multiple Car9 tags are able to oligomerize on the surface of nanoparticles creating a destabilizing shell, or just that multiple sfGFP-Car9 oligomerize in solution leading to this peak. Ultimately, these results are consistent with the FRET data of **Table 1** and reflects Car9-mediated protein adsorption to nanoparticles, with sfGFP::Car9 being more closely associated with RhSiNP than sfGFP-Car9.

In sharp contrast, addition of sfGFP::Car9-Car9 to RhSiNP at pH 7.5 led to a drastic increase in the distribution's mean D_h (to 1700 ± 450 nm), reflecting the formation of large protein-particle assemblies that settled at the bottom of the cuvette over time (**Fig. 2.1A**). The clustering of RhSiNPs through the bridging action of sfGFP::Car9-Car9 could also be visualized by SEM (**Fig. 2.1B**). Remarkably, shifting the pH to 8.5 by addition of sodium hydroxide caused near quantitative dissociation of the large assemblies into individual particles and small clusters whose size distribution matched that of protein-coated RhSiNP (**Fig. 2.1C and 2.1A**, light blue trace). Furthermore, it was possible to repeatedly cycle the particles between their assembled and

dissociated states by adjusting the pH of the solution between 7.5 and 8.5 (**Fig. 2.1A** and **2.1D**). Repeating the experiments with the sfGFP::Car9-K8AK11A variant led to the production of

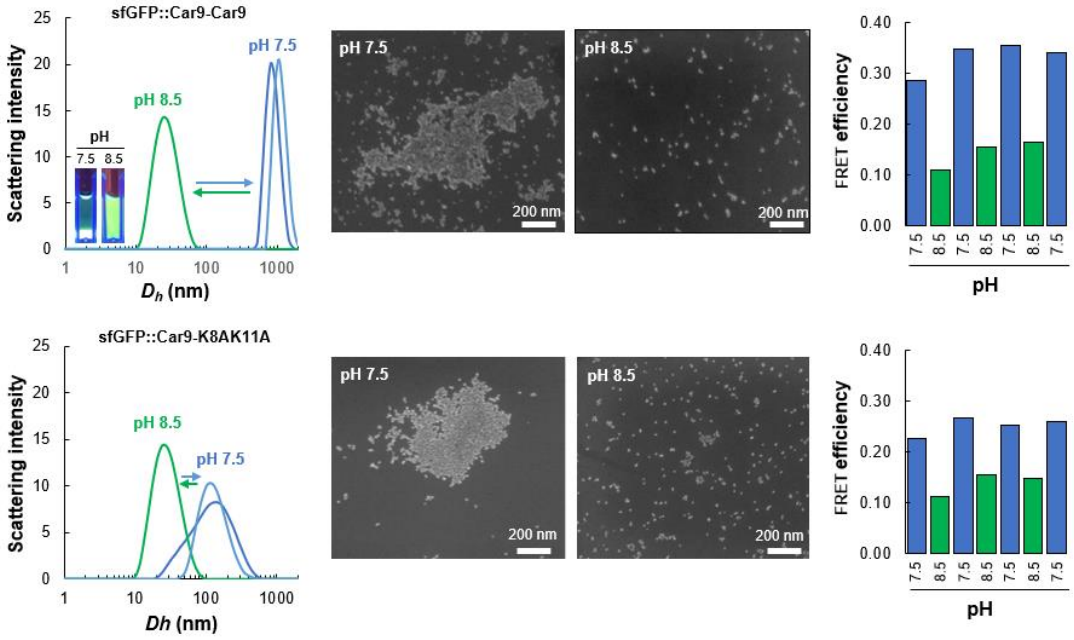

Figure 2.1 pH-controlled assembly and dissociation of RhSiNP particles using sfGFP::Car9-Car9 (A-D) or sfGFP::Car9-K8AK11A (E-H). Size distributions were acquired by DLS after incubating 5 µM of sfGFP::Car-Car9 (A) or 5 µM of sfGFP::Car9-K8AK11A (E) with 1 µM RhSiNP for 30 minutes at pH 7.5 (dark blue traces), after adjusting the pH to 8.5 (green traces) and after returning the solution to pH 7.5 (light blue traces). The inset of panel A shows the appearance of the solution at pH 7.5 or 8.5 under UV illumination and after 30 min incubation without mixing. Aliquots of samples prepared at pH 7.5 (B, F)) or pH 8.5 (C, G) were imaged by SEM. (D, E). FRET efficiencies were measured upon successive cycles of pH shifts. (Data for this figure was collected initially by Yundi Zhao and then replicates were completed by Julia Boese)

smaller assemblies with a broader size distribution and a mean D_h of 520 ± 350 nm (**Fig. 2.1E-F**). As was the case with sfGFP::Car9-Car9, these colloidal structures could be efficiently dissociated by increasing the pH to 8.5 (**Fig. 2.1E** and **2.1G**) and it was possible to use single-unit pH changes to cycle between assembled and dissociated states (**Fig. 2.1E** and **2.1H**).

To summarize, homobifunctional silica-binding proteins can be used to assemble RhSiNP into large supramolecular clusters at near neutral pH, cluster size can be controlled by the

identity/silica-binding affinity of the C-terminal SBP, increasing the pH by one unit resolves large assemblies into individual particles, and alternating the pH between 8.5 and 7.5 supports repeated cycles of particle assembly and disassembly.

2.3.3 Controlling protein-NP aggregate size by modulating solution and assembly conditions.

The ability to tune aggregate size is an important aspect of controlling and understanding this system, and within the buffering range of Tris HCl, we tested the average aggregate size formed from sfGFP::Car9-Car9 and 10nm RhSiNP (**Fig 2.2A**). The general trend is that larger aggregation of protein and RhSiNP occur at more acidic pH while above pH of 8.5 aggregation of the system no longer occurs and between pH 7.5 and pH 8 there is a stark change in the qualities of the solution

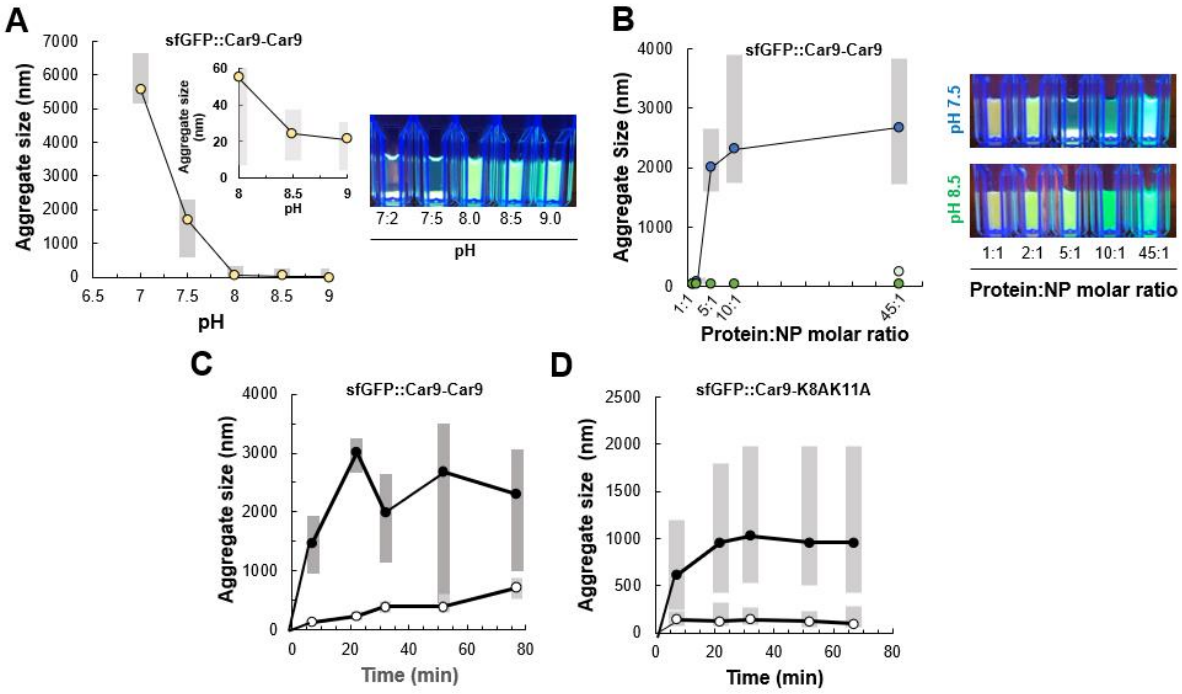

Figure 2.2 (**A**)Aggregate size of sfGFP::Car9-Car9 and RhSiNP as a function of the pH of the solution. Concentration of the RhSiNP is held constant at 1μM and the concentration of sfGFP::Car9-Car9 is 5μM. Solution conditions were 20mM Tris-HCl, and pH altered through addition of 1M NaOH or 1M HCl. (**B**) Aggregate size of sfGFP::Car9-Car9 and RhSiNP as a function of the protein molarity. Concentration of the RhSiNP is held constant at 1μM. Solution conditions were 20mM Tris-HCl, pH 7.5 (**blue**) and pH 8.5 (**green**). * notes where there were 2 peaks of relatively similar intensity. (**C**)Average aggregate size of sfGFP::Car9-Car9 and RhSiNP (**D**) and sfGFP::Car9-K8AK11A and RhSiNP. Black data points are the largest aggregate sizes measured by DLS and the white data points are the size of any secondary peaks.

with aggregates settling out of solution at the more acidic pH. Tuning the solution pH between pH 7.0 and pH 8.5 allows for full control of the association/dissociation behavior and allows for size control between protein coated dimer sized aggregates at 60nm and large aggregations of RhSiNP and protein measuring over 5000nm. These results are consistent with zeta potential and surface science theories, that state with more basic pH, zeta potential decreases, allowing colloidal dispersions to be more stable and less likely to aggregate.[70,71] To further support this, we measured the zeta potential of the RhSiNP at both a pH of 7.5 and 8.5 and found that the zeta potential of the neat RhSiNP are more negative at a pH of 8.5 than at pH 7.5 supporting the trends we see in aggregation (**Table 2, Fig. 2.3**). With the addition of protein to the system, at both pH 7.5 and pH 8.5 the zeta potential becomes more positive, which is consistent with the protein coating the RhSiNP at both pH 7.5 and 8.5 as is supported by the DLS data previously mentioned. At pH 8.5 the pure proteins, sfGFP::Car9-Car9 and sfGFP::Car9-K8AK11A, do not have a significant difference in zeta potentials (-9.5 ± 1.3 mV and -8.5 ± 2.3 mV, respectively), and the difference between each protein's zeta potential at pH 7.5 and pH 8.5 is also negligible ($P>0.1$).

At pH 7.5 there is a significant difference between the zeta potentials of the pure proteins, $P=0.02$, with sfGFP::Car9-Car9 having a zeta potential of -7.1 ± 0.5mV while sfGFP::Car9-K8AK11A is slightly more positively charged at -5.5 ± 0.8 mV. In the aggregated systems, RhSiNP@ sfGFP:Car9-Car9 aggregates have a more negative zeta-potential (-19.8 ± 1.1 mV) than the sfGFP::Car9-K8AK11A and RhSiNP aggregate counterpart at -16.6 ± 4.3, but with no significance between them. Both, however, show significantly different zeta potentials than the neat- RhSiNP at pH 7.5. At pH 8.5, there is no significant difference in the zeta potentials most likely due to the nanoparticles having fewer proteins coating the surface but further studies are needed to confirm. Furthermore, the only system with a significant zeta potential difference

between pH 7.5 and pH 8.5 is with the sfGFP::Car9-Car9 and RhSiNP system. This supports the DLS data that shows sfGFP::Car9-Car9 creating larger aggregates than sfGFP::Car9-K8AK11A since the change in double layer is actually significant in this system.

Since most systems are concentration dependent, we wanted to understand the role of

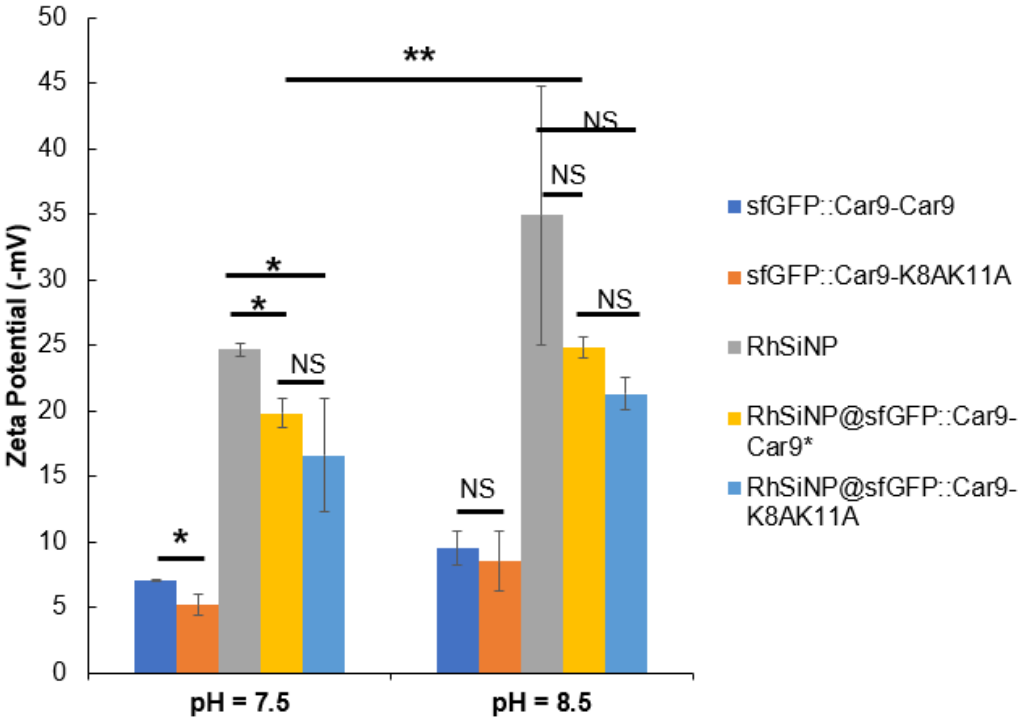

Figure 2.3: Zeta potentials for each protein and protein-NP combination at pH 7.5 and pH 8.5. * denotes significance ($p < 0.05$) between different proteins at the same pH, ** denotes significance between pH with the same protein, and NS denotes no significance.

protein concentration on the ability for the system to aggregate and on the aggregate size. For sfGFP::Car9-Car9, increasing protein concentration increases the size of aggregates up to an approximate maximum of 2700 nm (**Fig. 2.2 B**). Below a protein to RhSiNP ratio of 5:1, aggregates cannot assemble to a size that allows them to settle out of solution (**Fig. 2.2B Photo insert**). Furthermore, at higher concentrations such as the 45:1 ratio, complete disassembly does not occur and a secondary peak at about 220 nm is present. Since there is excess protein in the system, it is likely that these 220nm aggregates consist of excess protein due to Car9's

oligomerization capabilities, or that with excess protein there are enough surface bound sfGFP::Car9-Car9 to continue to bridge other nanoparticles even at pH 8.5. Important notes about the figure 2.2B insert for the 10:1 and 45:1 mixtures, even though there looks to be a smaller amount of aggregates settles at the bottom of the cuvette, this is due to a lower concentration of protein and NP (2μM and 0.2μM for the 10:1 ratio and 9μM and 0.2μM for the 45:1 ratio) due to the concentration of nanoparticles offered by the manufacturer. This difference in NP and protein concentration is shown to not affect the behavior of the system as it seems to be solely dependent on the ratio between protein and NP, not the concentration of both reagents, with lower concentration mixes reaching average sizes of 1900nm and 520nm for sfGFP::Car9-Car9 and sfGFP::car9-K8AK11A aggregates respectively (**Fig A.4)**.

Elucidating the kinetics of the system was also important to controlling the aggregation formation size, so time-dependent aggregation studies were completed on both sfGFP::Car9-Car9 and sfGFP::Car9-K8AK11A systems with 10nm RhSiNPs (**Fig, 2.2C and D**). The sfGFP::Car9-Car9 and 10nm RhSiNP aggregates are polydisperse with two main peaks at each time point. The larger of the two levels out at approximately 2500 nm starting at 30min and the smaller peak continues to grow as time continues. The sfGFP::Car9-K8AK11A achieves a much smaller maximum size settling at about 1000 nm beginning at 30 min. The secondary peak is also much smaller for the sfGFP::Car9-K8AK11A system as it caps immediately at about 200 nm. The kinetics data supports the DLS and FRET data previously reported and shows how the mutations to the Car9 tag decrease the aggregate size and also how the kinetics of aggregation are on a relatively similar timescale for both systems.

DLVO theory states that the addition of ions will shield surface charge, leading to more positive zeta potential, and less stable colloidal systems or increased aggregation.[59] In order to further gain control over the size of the aggregates formed. **Figure 2.4A ,C** shows that the addition of NaCl into a 10nm RhSiNP and sfGFP::Car9-Car9 system allows for increasing aggregate size at a pH of 7.5, reaching a maximum size of approximately 4100 nm after 30 min for NaCl concentrations above 25mM. This is much larger than the 1700nm aggregate size recorded at

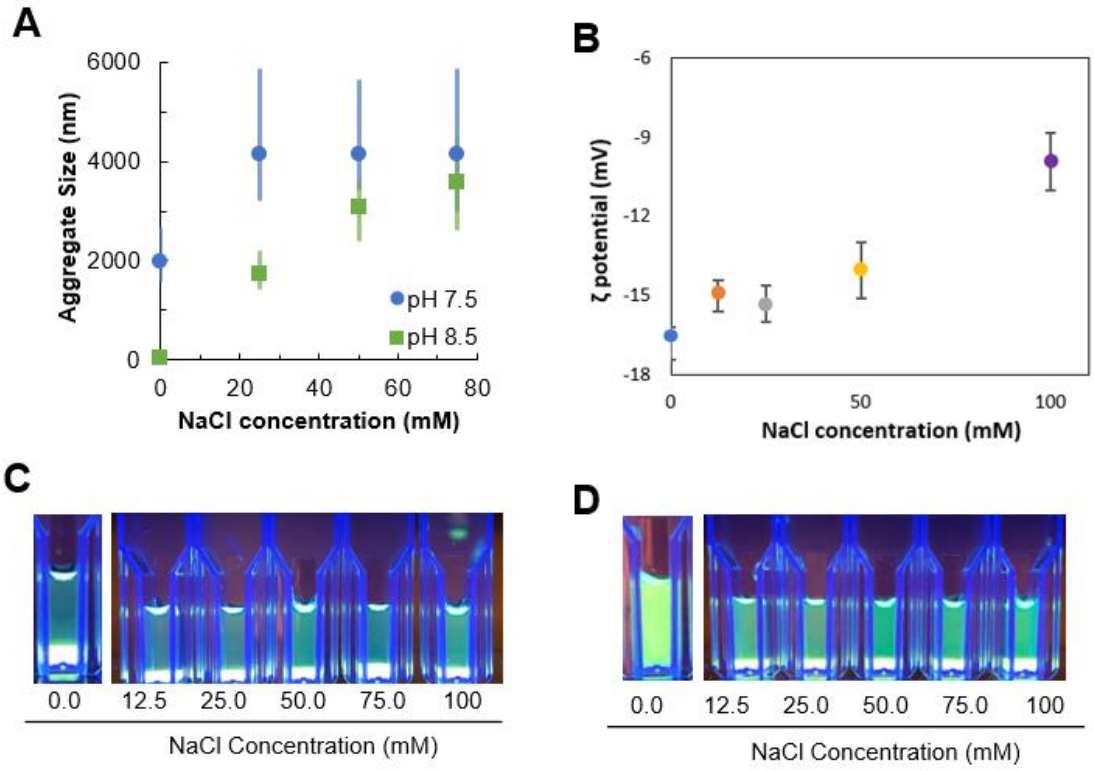

Figure 2.4. (**A**) Aggregate size of sfGFP::Car9-Car9 and RhSiNP as a function of the NaCl concentration. Concentration of the 10nm RhSiNP is held constant at 1μM and protein held at 5μM. Solution conditions were 20mM Tris-HCl, pH 7.5 (Blue) or pH 8.5 (Green) with NaCl concentration as listed. Error bars denote full width at half max to denote polydispersity of each average aggregate size. (**B**) Zeta potential of each solution condition (Data collected by Yundi Zhao). The bottom panels show sfGFP::Car9-Car9 and RhSiNP aggregates in, or settling out of solution, after 30 minutes of mixing at pH 7.5 (**C**), and pH 8.5 (**D**).

0mM NaCl, a trend supported by DLVO and double layer theory and by the zeta potentials measured for the system (**Fig. 2.4B**). The more interesting aspect of this system is that with the addition of salt, the system is more prone to aggregate and the higher NaCl concentrations

stabilized the aggregate size in the disassembly process. As the NaCl concentration increases, the larger the aggregates are, even at pH 8.5. **Fig 2.4D** shows that increasing the NaCl concentration allow protein-NP aggregates to remain large enough to precipitate out of solution even though there seems to be an increased amount of free protein in solution at pH 7.5 compared to pH 8.5 (**Fig. 2.4C-D**), due to the aggregates partially dissociating, even with higher NaCl concentrations. An important note regarding the data include that at 100mM NaCl, the DLS data quality was always too poor to receive accurate readings of the aggregate size possibly due to interference of the NaCl with the reading.

Clearly, aggregate size and disaggregation efficiency can be tuned by altering solution conditions such as ion concentrations or 'reactant' concentrations, changing the amount of time the solution is allowed to react, or changing the identity and properties of the solid-binding peptide. With this understanding, it was important to be able to achieve some predictive ability in assembling species with slightly different surfaces or sizes of nanoparticles.

2.3.4 Expanding this knowledge base to different SiNP surfaces and sizes.

We know that aggregation of these nanoparticles by dual-tagged sfGFP is concentration dependent, with lower concentrations of proteins hindering NP aggregation. With this in mind, we predicted that a 5:1 ratio of protein to 30nm RhSiNP would not aggregate because of the increased surface area of the 30nm RhSiNP compared to the 10nm RhSiNP. In a 5:1 protein to RhSiNP mix, aggregates did not assemble at pH 7.5 (**Fig. 2.5A**) but upon increasing the ratio of protein to RhSiNP to account for the 9-fold increase in surface area, aggregates assemble to 2150 ± 220 nm and are visible to the naked eye as increased turbidity (**Fig. 2.5B**). This system retains the ability

to disaggregate at pH 8.5, as well as the ability to be cycled between aggregated and dissociated states (**Fig. 2.5B-C**).

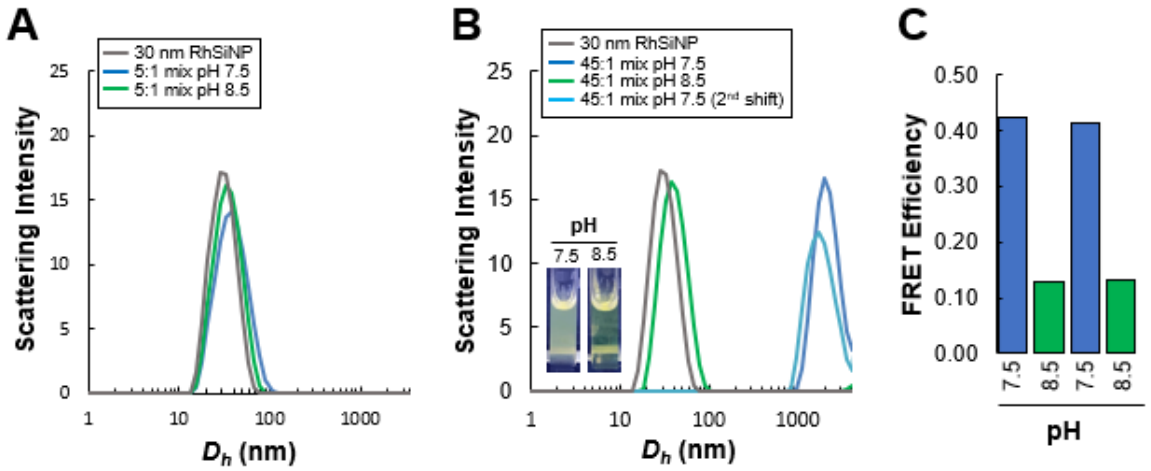

Figure 2.5. (**A**) Size distribution of 1µM 30nm RhSiNP system with 5µM sfGFP::Car9-Car9 **(B)** Size distribution of 1µM 30nm RhSiNP system with 45µM sfGFP::Car9-Car9 with the insert depicting the protein and RhSiNP solution 30 min after mixing at pH 7.5 and 3 min after switching to pH 8.5 (**C)** FRET efficiency of sfGFP::Car9-Car9 -30nm RhSiNP samples.

Furthermore, Puddu et al. has shown that increasing NP size makes zeta potential more negative and more stable.[51,61] We measured the zeta potential of the 30nm RhSiNP (**Fig. 2.6A**) to see if the difference in protein concentration needed to aggregate these nanoparticles was due to some surface difference. We see that the difference in zeta potential between the 10nm and 30nm RhSiNP is significant at both pH 7.5 and pH 8.5 (P= 0.02 and P= 0.01respectively) (**Table 2, Table 3**). Within the 30nm RhSiNP, there is a negligible difference between the zeta potentials at pH 7.5 and pH 8.5 and even with the addition of protein at pH 7.5 there is no significant difference between the system with protein and the neat RhSiNP system **(Fig. 2.6A)**. Similarly, there is no significant difference in zeta potentials within the pH 8.5 category. Taken together this shows that the addition of protein does not alter the surface charge with the increased surface area, unlike the

protein altering the zeta potential of 10nm RhSiNP at pH 7.5. The only significant change (P<0.05)

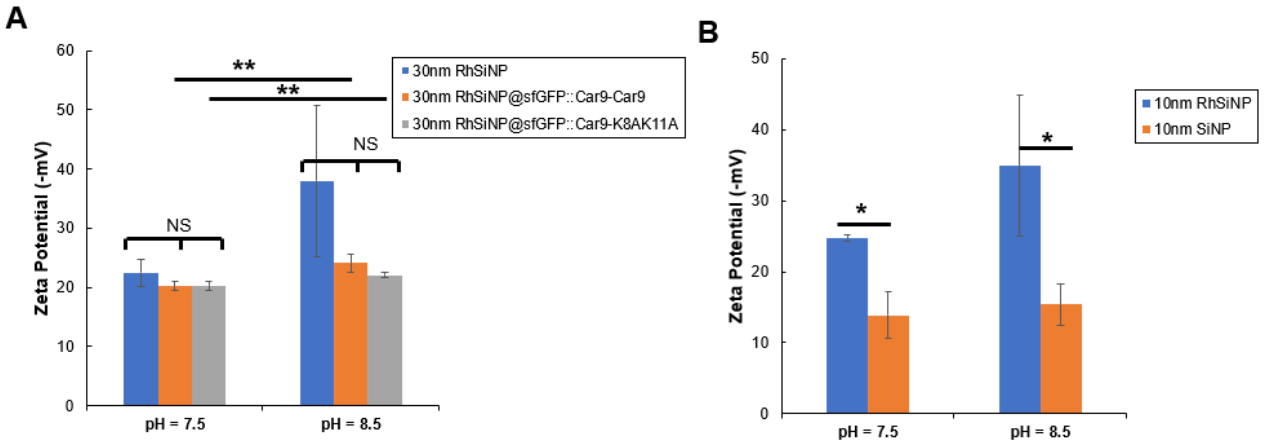

Figure 2.6: (**A**) Zeta potentials for each protein and protein-30nm RhSiNP combination at pH 7.5 and pH 8.5. (**B**) Zeta potentials for each sfGFP::Car9-Car9-10nm SiNP compared to sfGFP::Car9-Car9-10nm RhSiNP mixtures at pH 7.5 and pH 8.5. * denotes significance within a pH and between systems (P <0.05), ** denotes significance (P<0.05) between different pH in the same system, and NS denotes no significance.

in zeta potential with the 30 nm RhSiNP was between the NP systems with protein at differing pH. For both sfGFP::Car9-Car9 and sfGFP::Car9-K8AK11A, increasing the pH decreased the zeta potential significantly, as is supported by both the disaggregation of the system and the double layer theory. Taken together with the RhSiNP not aggregating at pH 8.5 alone (**Fig. A. 3-A.5**), this supports that the protein is causing the association of the RhSiNP. Although we are relatively certain that the Rhodamine dye is encapsulated within the RhSiNP as per the manufacturer, we measured the zeta potential of the SiNP to determine if the surface charges were similar. The surface charge of the 10nm RhSiNP was significantly more negative than the 10nm SiNP at pH 7.5 (-24.7 ± 0.5 mV and -13.9 ± 3.2 mV respectively) and pH 8.5 (-34.9 ± 9.9 mV and 15.4 ± 2.9 mV respectively) (**Fig. 2.6B)**. Hence, we predicted that the 10nm SiNP would be more prone to aggregation with the addition of protein than the 10nm RhSiNP under the same conditions. To our surprise, the 10nm SiNP did not aggregate upon addition of sfGFP::Car9-Car9 at a 5:1 protein to

SiNP ratio(**Fig. 2.7A**). Once the protein concentration was increased to a 10:1 sfGFP::Car9-Car9: SiNP ratio, aggregation and dissociation returned for the system (**Fig. 2.7B**).

At both the 5:1 sfGFP::Car9-Car9 and 10nm SiNP solution at pH 7.5 and the 10:1 sfGFP::Car9-Car9 and SiNP solution at pH 8.5, there was some aggregation sizing 400nm. This could be due to either aggregation of sfGFP::Car9-Car9 or aggregation of the SiNP due to their more positive zeta potential, although the pure 10nm SiNP do not aggregate at pH 7.5 or pH 8.5,

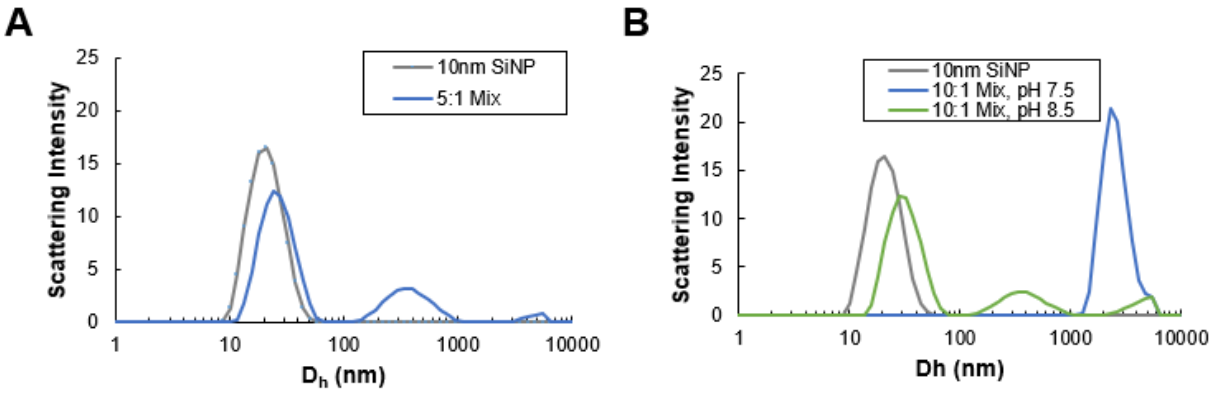

Figure 2.7: (**A**) Size distribution of 1 µM 10nm SiNP system with 5 µM sfGFP::Car9-Car9. (**B**) Size distribution of 1µM 10nm SiNP system with 10µM sfGFP::Car9-Car9.

(**Fig A.4 B**). Strangely enough, sfGFP::Car9-K8AK11A does not aggregate at either a 5:1 or 10:1 ratio of protein to 10nm SiNP but small aggregates similar to those seen in the SiNP and sgGFP::Car9-Car9 system at about 400nm are present(**Figure A.6**). More investigation needs to be completed as to why this is occurring.

2.4 Conclusions and Future Directions

FRET[63,66], DLS and zeta potential[69,70] measurements are mature techniques in the colloidal field and are utilized here to examine the separation, size, and surface characteristics of Car9 fusion proteins and RhSiNPs as both systems and components. While sfGFP and Rhodamine are not an ideal FRET pair given the small overlapping area in their spectra compared to popular FRET materials such as CFP and YFP[63] and the multiple donors and acceptors in our system make

determining exact distances impossible[63,66], we have shown here that this donor-acceptor pair is very valuable to capture the binding behavior of Car9 variants as a function of solution pH. It should be broadly useful in the future to study protein-mediated assembly of NPs even in scenarios with multiple donors and acceptors.

Motivated by the challenge of controlling the assembly of nanoscale materials in a precise and flexible fashion, here we focused on using bifunctional solid binding proteins tagged with the Car9 silica binding peptide to build a dynamic protein-nanoparticle system in which assembly - disassembly behavior can be controlled by changing solution condition (e.g pH and salt concentration) and components (eg protein tag and SiNP size and surface composition). Interactions between Car9 and the silica interface and its ability to oligomerize are previously described and reliant on electrostatic interactions between the positively charged lysine and arginine residues in Car9 and the negatively charged silanol groups on the silica surface and well as its structure.[35,43,48,49]

Our results indicate that the difference in silica binding capabilities of Car9 and its variants lends itself to differences in aggregation sizes since larger aggregates were formed by the homobifunctional sfGFP::Car9-Car9 than the semi-homobifunctional sfGFP:Car9-K8AK11A. Both systems allow for decomposition of the aggregates by a simple shift of one pH unit and the process is reversible. We also show that control of assembly size and disassembly can be achieved by changing the NaCl concentration. We observed an increase in aggregate size with the NaCl concentration paired with a decrease in the ability for aggregates to dissociate. This model follows what is proposed in DLVO theory and electrical double layer theory,[57] for colloidal solutions.

By synthesizing homobifunctional solid binding proteins with different binding behavior, we have developed a novel approach to manipulate the aggregation and disaggregation of silica

nanoparticles using small changes in solution alkalinity. We have further shown that aggregate size is tunable by changing SBP composition, reagent concentrations, equilibrium time, salt concentration, and NP size. Achieving dynamic control of nanoparticle assembly with computationally designed proteins is the next frontier for the predictive production of hierarchical architectures useful in biomedicine, biomaterial fabrication and energy devices. We expect that a detailed understanding of the kinetics of assembly and disassembly using real-time imaging coupled with simulations and experiments will go a long way towards this goal. We also expect that hyperspectral microscopy will be able to help us determine the exact composition of unknown smaller aggregates.

Chapter 3 Protein Valency

3.1 Introduction

Previously, we reported on the use of homobifunctionally Car9-tagged derivatives of sfGFP to assemble RhSiNPs at pH 7.5 while maintaining reversibility between assembled and disassembled states by tuning the pH between pH 7.5 and pH 8.5.[53] We were further able to control the size of the aggregates and their ability to form by altering tag variation (Car9 versus K8AK11A), ion concentration, and protein concentration.[53] Based on previous reports, the size of the NP in comparison to the linker molecule is integral to both assembly and control of the crystal structure of the linked-NP formations.[39,72] In order to breach this gap between sfGFP (4nm by 2nm beta-barrel) and the 10nm RhSiNPs, a group of *de novo* proteins developed by Fallas et al. that were more closely sized to the 10nm RhSiNPs (approximately 7nm by 7nm) and had cyclic repeats allowing for extension of the size of the protein monomers were explored for silica binding capabilities.[73] A heat stable, tetrameric glucokinase (GK) from *Bacillus stearothermophilus* was used to further explore the size of protein linker in conjunction with NP size.[74]

Here, we combine DNA manipulations and DLS to explore a variety of different multi-valent *de novo* and native proteins in which to expand the protein mediated RhSiNP assembly. Additionally, we explore how the use of these proteins could lead to more organized patterning of the protein-NP assemblies.

3.2 Materials and Methods

3.2.1 DNA manipulations and protein purification. Plasmid pET24a(+)- sfGFP which encodes a derivative of superfolder green fluorescent protein (sfGFP)[43] was cut at *XbaI* and *XhoI* digestive sites to obtain the backbone for each of the proteins used. pET24a(+)-GK-Car9 and pET24a(+)-GK were described previously[48] and encode for a Car9-tagged glucokinase and an untagged glucokinase protein.

Oligomers were ordered for each *de novo* protein including 20-30 bp overhangs for the pEt24a(+) plasmid in order to complete assembly through Gibson Assembly (Sequences used are included in Appendix B). Plasmid pET24a(+)-Ank1C2_1 encodes Ank1C2_1 and plasmid pET24a(+)-Ank3C2_1 encodes Ank3C2_1, two dimers developed previously.[73] Plasmid pET24a(+)-1na0C3_3 encodes 1na0C3_3 and plasmid pET24a(+)-HR00C3_2 encodes HR00C3_2, two trimers developed previously.[73] Plasmid pET24a(+)-Ank1C4_1 encodes Ank1C4_1 and plasmid pET24a(+)-Tj10C4 encodes Tj10C4, two tetramers developed previously.[73] The integrity of all constructs was verified by DNA sequencing and plasmids were introduced into *E. coli* BL21(DE3).

For the Car9 tagged versions of the *de novo* protein oligomers were ordered to encode for each protein and insert into pET24a(+)-sfGFP between *XbaI* and *XhoI* digestive sites. Ank1C2_1 and Tj10C4_G1 had surface accessible N-termini so Car9-Ank1C2_1 and Car9-Tj10C4_G1 proteins were encoded into pET24a(+)-Car9-Ank1C2_1 and pET24a(+)-Car9-Tj10C4_G1 plasmids respectively. These two proteins were designed with a GGGS linker, TEV site, and additional MG amino acids to encode a NcoI digest site into the protein. Ank3C2_1-Car9, HR00C3_2-Car9, Ank1C4_1-Car9 and 1na0C3_3-Car9 proteins were encoded into pET24a(+)-Ank3C2_1-Car9, pET24a(+)-HR00C3_2-Car9, pET24a(+)-Ank1C4_1-Car9. and pET24a(+)-1na0C3_3-Car9 respectively. The c-terminally tagged proteins were designed with a KLGGGS linker between the last amino acid of the main protein and the Car9 tag, introducing a HindIII site.

Car9-expressing cultures for both GK and *de novo* proteins were grown and induced, and proteins purified by silica affinity purification as described.[43,46] GK was purified from BL21(DE3) cells harboring pET24a(+)-GK by Fast Protein Liquid Chromotagraphy (FPLC) using a BioRad DEAE ion exchange chromatography column. The protein was loaded onto the column and

washed using Tris-HCl, pH 7.5 and eluted using a gradient elution with 20mM Tris-HCl, 1M NaCl, pH 7.5. Protein were concentrated to about 50mg/mL in 20mM Tris-HCl, pH 7.5 using an Amplicon microconcentrator, aliquoted, and stored at -20C. Untagged versions of the *de novo* proteins were purified from BL21(DE3) by Fast Protein Liquid Chromotagraphy (FPLC) using a BioRad DEAE ion exchange chromatography column. An optimized process for purifying these untagged proteins was not completed during my time in the lab.

3.2.2 pH cycling for protein-NP solutions. The rhodamine-conjugated silica nanoparticles (RhSiNP) terminated with surface silanols,10nm diameter, and concentrated to 25 mg/mL were purchased from Micromod Partikeltechnologie GmbH (Rostock, Germany). To assess the affinity of GK and GK-car9 with silica, protein and nanoparticle were mixed to a final concentration of 5μM or 3 μM protein (calculated per monomer) and 1μM RhSiNP in 20mM Tris-HCl, pH 7.5. The final volume of the mixed solution was between 500μL and 3mL and were stored in either a 2mL Eppendorf tube or a 15mL capped-conical tube. The protein-NP solutions were then mixed on a tube rotator for 30 minutes before acquisition of, FRET, DLS, or ζ-potenital. For pH cycling experiments, samples were prepared and data collected as stated above. Samples were then treated with 1M NaOH added in 1 μL increments and after each addition the tube was inverted 4-6 times prior to pH measurement with a Mettler Toledo microtip pH electrode. Once the solution reached pH 8.5, the tube was placed on a tube rotator for 30 minutes before data acquisition. To acidify the solution back to pH7.5, 1M HCl was added in the same quantity used to alkalize the solution and then the tube was placed on a tube rotator for 30 minutes prior to data acquisition. Throughout acidification and alkalization process an average of 5mM Na^+ or 5mM Cl^- is added per cycle while a maximum of 10mM Na^+ or 10mM Cl^- is added to the solution per cycle.

3.2.3 Analytical Techniques. A Zetasizer Nano ZS (Malvern Instruments) was used to monitor NP and protein sizes and the formation of aggregates. Measurements comprising 12-20 measurement cycles were performed on 500µL of samples prepared in three independent experiments. Zeta potentials were measured on the same instrument using folded capillary cells (DTS1070, Malvern Instruments).

3.3 Results and Discussion

3.3.1 Using GK and GK-Car9 to assemble RhSiNPsAnalytical Techniques. In previous work we used homobifunctional derivatives of sfGFP with dual Car9 silica-binding peptides genetically installed at the C-terminus and within permissive loop 9 (sfGFP::Car9-Car9) or a variant inserted into the C-terminus (sfGFP::Car9-K8AK11A) to assemble RhSiNPs and SiNPs under varying solution conditions.[53] We used DLS to probe assembly and disassembly of these NPs under two conditions of pH (7.5 and 8.5). To expand our knowledge of this system we designed a Car9 tagged homotetramer GK-Car9 which when fully assembled into its tetrameric state, presents 4 Car9 tags

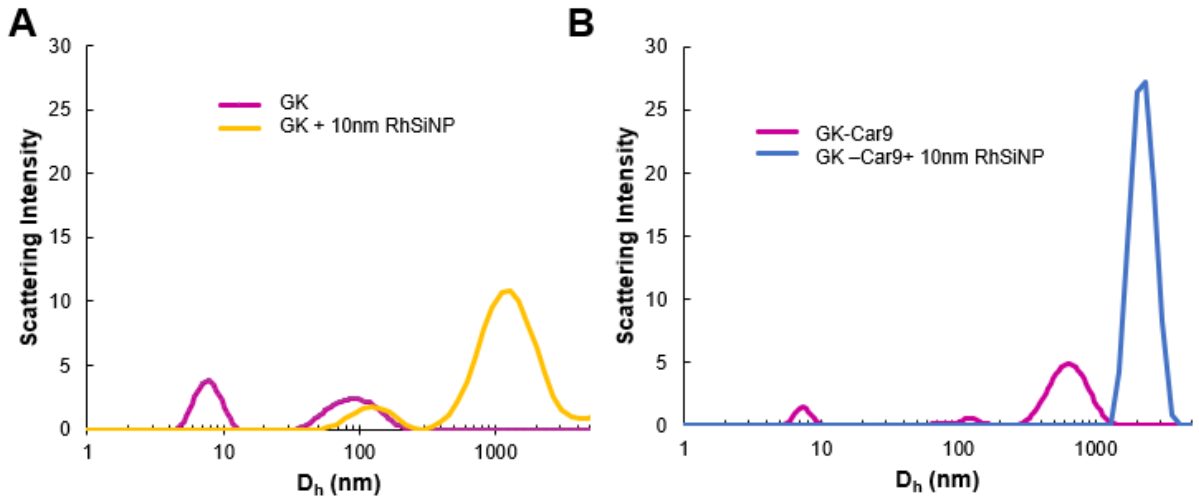

Figure 3.1. (**A**) Size distribution of 5µM GK (pink) and GK and 10nm RhSiNP system (yellow) with 5 µM GK and 1µM 10nm RhSiNP in 20mM Tris HCl, pH 7.5. (**B**) Size distribution of 5µM GK-Car9 (pink) and GK-Car9 and 10nm RhSiNP system (blue) with 5µM GK-Car9 and 1µM 10nm RhSiNP in 20mM Tris HCl, pH 7.5.

per protein and one Car9 per monomer (**Fig. B.1**). GK-car9 assembles in our solution conditions,[48]

although there is a possibility that some monomers and dimers of GK-Car9 will not fully assemble to their tetrameric state, meaning there may be some heterogeneity in the protein solution. Knowing that GK is most stable at pH 8.5,[74] and to show that GK and GK-Car9 did not aggregate in solution without RhSiNPs present, we completed DLS measurements at a pH of 7.5 (**Fig 3.1**). Here we see that pure GK does not aggregate fully and its hydrodynamic diameter nominally measures at 9nm with a secondary peak of aggregates measuring 80nm, while the majority of intensity measured from the GK-Car9 sample shows aggregates measuring 650nm with a smaller amount of intensity denoting protein measuring 9nm. Since larger particles and aggregates scatter light more intensely than smaller aggregates in a manner consistent with D^6, we looked at the simplification of the data that tries to account for this difference by converting intensity to number

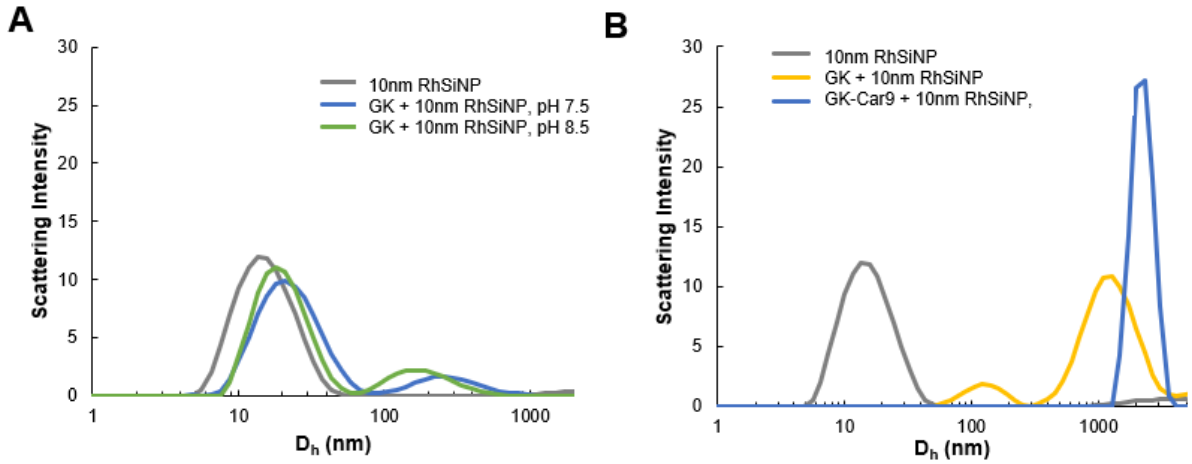

Figure 3.2.(**A**) Size distribution of 1µM 10nm RhSiNP (grey) or GK and 10nm RhSiNP system with 3 µM GK and 1µM 10nm RhSiNP in 20mM Tris HCl, pH 7.5 (blue) and pH 8.5 (green). (**B**) Size distribution of 1µM 10nm RhSiNP (grey) or GK and 10nm RhSiNP system (yellow) with 5 µM GK and 1µM 10nm RhSiNP and the GK-Car9 and 10nm RhSiNP system (blue) with 5µM GK-Car9 and 1µM 10nm RhSiNP in 20mM Tris HCl, pH 7.5.

of particles (**Fig B.2**). When looking at the DLS spectra calculated to take into account the larger aggregates scattering more, one can see most of the pure GK and pure GK-Car9 remain unaggregated in solution. Using both the intensity and number measurements (**Fig. 3.1** and **Fig. B.2A,B**) show that upon the addition of the 10nm RhSiNP both systems aggregate to 1200nm and

2000nm for GK and GK-Car9 respectively. To further explore this we decreased the concentration of GK to 3μM and looked at if, upon the addition of 10nm RhSiNP, the system aggregated (**Fig 3.2A**). At the lower protein concentration, the system did not aggregate without the Car9 tags included. Additionally, we tried to purify GK on silica resin as described for the GK-Car9 proteins, and at least at the size of the silica resin, there was no interaction between the protein and silica. Returning to 5μM protein mixed into solution, GK assembles smaller RhSiNP aggregates than GK-Car9 which is supported by fact that Car9 is used to bridge silica in previous studies (**Fig. 3.2B**).[53] Overall, the reason as to why untagged GK was able to assemble RhSiNPs in solution was not determined but since GK is an enzyme with an active site, there is a possibility that SiNPs match the charge of surface chemistry of the enzymatic active site, leading to GK-silica associations.

3.3.2 Use of *de novo* proteins to assemble NPs. The *de novo* proteins were designed as both untagged and tagged versions and after the first purification of the untagged proteins, there were no proteins that remained stable in solution. These proteins will need to be re-expressed and purified in future work while working to optimize the purification process without adding salt or other stabilizing reagents (glycerol) that may affect the binding kinetics and abilities with silica and SiNP.

3.4 Conclusions and Future Directions

Motivated by the challenge of controlling the assembly of nanoscale materials in a precise and flexible fashion, here we focused on using multimeric solid binding proteins tagged with the Car9 silica binding peptide to build a dynamic protein-nanoparticle systems from components more equal in size. This work lays the groundwork for all future experiments using the Car9-tagged *de novo* and GK proteins. Preliminary results indicate that working with multimeric proteins may

be more difficult than we imagined and that a lot of work will go into determining why certain proteins may interact with nano-particulate silica as opposed to traditional silica resins. Furthermore, purifying the *de novo* proteins and keeping them stable in solution without salt or glycerol may prove difficult, and prior to experimenting with SiNP, we know that we should screen the untagged *de novo* proteins for silica binding capabilities prior to introducing the Car9 tags.

Chapter 4 With QDs and MSCs

4.1 Introduction

Previously, we reported on the use of homobifunctionally Car9-tagged derivatives of sfGFP to assemble RhSiNPs.[53] We were further able to introduce stimuli dependent aggregation and control of the aggregate size by altering tag variation (Car9 versus K8AK11A), ion concentration, pH, and protein concentration.[53] In addition to the use of SiNP in these types of systems, we have an interest in expanding our knowledge of solid-binding peptides and protein chemistry to link quantum dots (QDs) and magic-sized clusters (MSCs). Since QDs have semiconductor capabilities and size dependent optical properties,[75] introducing them into protein-linked nanomaterials could endow the materials with electronic properties and optical properties not offered when using silica. Furthermore, since the surface chemistries of QDs can be tailored to suit the needs of the function and the SBP or chemistry in use, these materials make for an interesting building block for protein-linked nanomaterials. Here, we manipulate DNA to create a variety of different proteins capable of binding to cysteine-capped CdSe or ZnS-coated InP quantum dots for use in future experimentation.

4.2 Materials and Methods

4.2.1 DNA manipulations and protein purification. Plasmid pET24a(+)- sfGFP which encodes a derivative of superfolder green fluorescent protein (sfGFP)[43] was cut at *XbaI* and *XhoI* digestive sites to obtain the backbone for each of the proteins used. pET24a(+)-sfGFP-CT43 was described previously[35] and encode for a c-terminally tagged sfGFP with ZnS binder CT43. Plasmids pET24a(+)-sfGFP::CT43 and pET24a(+)-sfGFP::CT43-CT43 encode sfGFP::CT43, containing the CT43 sequence within a permissive loop described previously, and sfGFP::CT43-CT43, a derivative of sfGFP-CT43 with an additional CT43 tag introduced within the same permissive loop

as sfGFP::CT43. Oligomers were ordered for each of these proteins and assembled into pET24a(+) between *XbaI* and *XhoI* digestion sites. These sequences are listed in Appendix C.

For the cysteine-modified sfGFP, oligomers were ordered to encode for each protein and insert into pET24a(+)-sfGFP between *XbaI* and *XhoI* digestive sites. Single binding variations of cysteine-mutated sfGFP included sfGFP(R2C C48S) and sfGFP(C48S G51C) which both included a mutation of free cysteine in the 48 amino acid to serine as is consistent with conservative mutations in most proteins.[76] Additional single binding variations included sfGFP(R2C C48S C70V) and sfGFP(C48S G51C C70V) which accounted for the possibility that the cysteine at position 70 may be surface accessible and that a cysteine-valine mutation at position 70 is conservative this close to the chromophore.[76] Dual binding variations include sfGFP(R2C C48S G51C) and sfGFP(R2C C48S G51C C70V). Each protein was cloned into pET24a(+) and named based on the protein encoded.

All proteins were purified from BL21(DE3) cells harboring each individual plasmid by Fast Protein Liquid Chromotagraphy (FPLC) using a BioRad DEAE ion exchange chromatography column. The protein was loaded onto the column and washed using Tris-HCl, pH 7.5 and eluted using a gradient elution with 20mM Tris-HCl, 1M NaCl, pH 7.5. Proteins were concentrated to about 50mg/mL in 20mM Tris-HCl, pH 7.5 using an Amplicon microconcentrator, aliquoted, and stored at -20C.

4.3 Results and Discussion

Both sfGFP::CT43 and sfGFP::CT43-CT43 proteins were expressed and purified for use with the ZnS-capped InP QDs (**Fig. C.1**). Four of the six cysteine-mutated proteins were expressed and purified including sfGFP(C48S G51C), sfGFP(R2C C48S C70V), sfGFP(R2C C48S G51C), sfGFP(R2C C48S G51C C70V) for use with the cysteine-capped CdSe QDs (**Fig. C.2**). A

preliminary study was completed to see if the fluorescence of sfGFP was different with amino acid 70 being changed as well as being close to the chromophore and the valine mutation did not

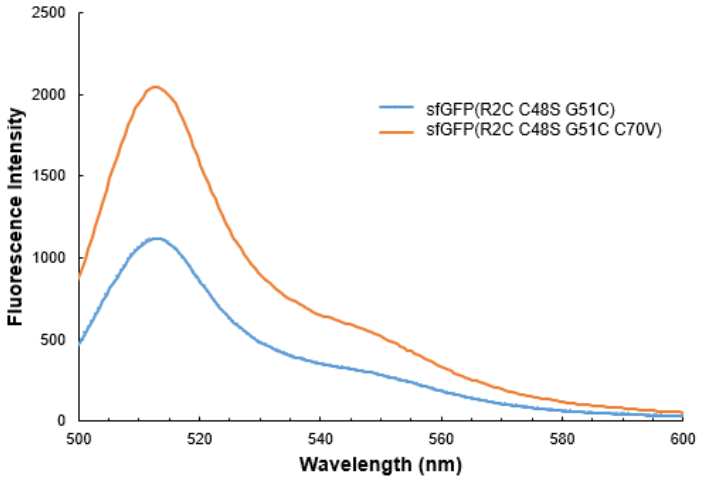

Figure 4.1 Fluorescence spectra of sfGFP (R2C C48S G51C) and sfGFP (R2C C48S G51C C70V) with excitation at 485nm.

negatively affect the fluorescence of sfGFP (**Fig. 4.1**). If anything it seemed to increase the fluorescence of the system which is highly unlikely based on existing data and understanding of mutations around the chromophore.[76] These experiments need to be completed again, in triplicate, before any further discussion can be made on the matter.

4.4 Conclusions and Future Directions

Motivated by the challenge of integrating complex materials into organized assemblies in a precise and flexible fashion, here we focused on designing homobifunctional ZnS binging and cysteine binding proteins to build a protein-QD systems. This work lays the groundwork for all future experiments using the ZnS and cysteine mutated sfGFP to integrate with various QDs.

Chapter 5 Conclusions

In this work we have employed a combination of experiments to understand how proteins can be used to bind SiNPs under a variation of solution conditions. We further investigated the expansion of this system to different multimeric proteins and to QDs. In Chapter 2, we used DLS and FRET to characterize the assembly and disassembly of protein-NP aggregates under different pH. We developed a method of aggregating RhSiNP and SiNPs at pH 7.5 and disassembling them by increasing the solution pH to pH 8.5. We further investigated the use of different Car9 mutations (K8AK11A), NaCl ions, pH, and protein concentration to control the size of aggregates and their ability to disassemble at pH 8.5. In Chapter 3, we began to expand the use of this system by designing multimeric *de novo* and native proteins with multiple Car9 tags and testing GK-Car9 in its ability to assemble NPs. Chapter 4 focuses on designing proteins for use in pattering cysteine-capped CdSe and ZnS-coated InP quantum dots. Further work on the work started in Chapters 3 and 4 is planned for future students in the lab.

The approaches and fundamental understanding developed in this work provide a roadmap that can be applied to organizing protein-NP assemblies as well as applied to other technologically useful SBPs. For instance, the ability to use FRET with multiple donors and acceptors as a way to determine overall assembly of a system can be applied to many cases where FRET has not been applied before. Additionally, understanding the conditions for protein-NP assembly can be used to improve methods of colloidal assembly for NPs and expand the function of colloidal and NP hierarchical materials. This work lays the ground-work of the broader goal of installing SBPs within computationally designed scaffolds for controlled assembly of hierarchal structures and the production of advanced materials and devices, with applications in fields as varied as biomedical engineering, catalysis, and opto-electronics.[4,5,10,77]

Appendix A. Supplementary Information for Chapter 2

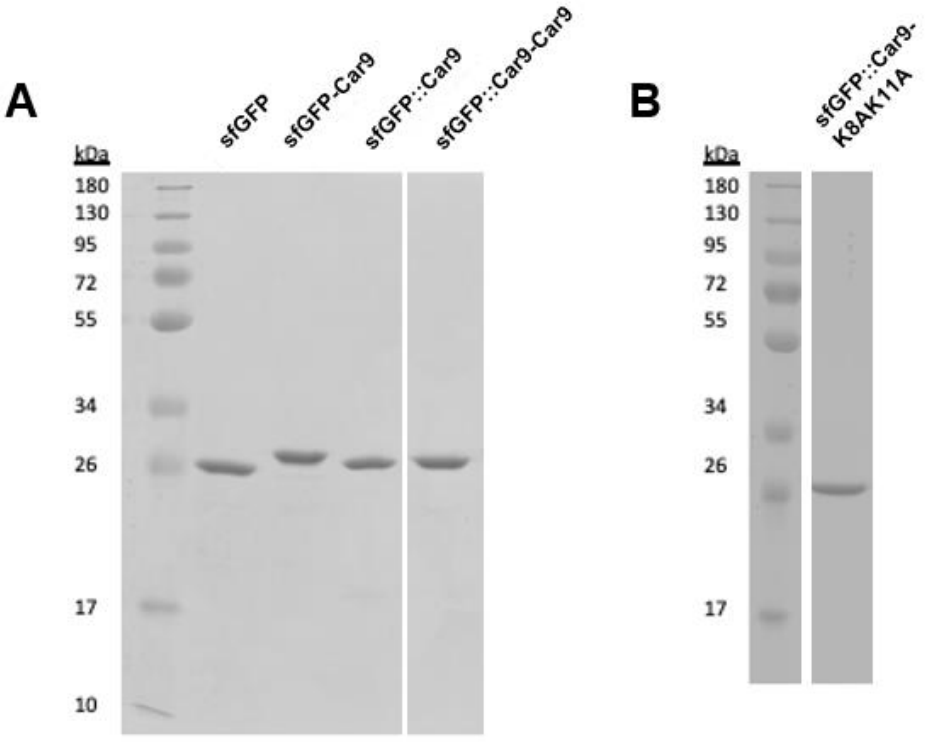

Figure A.1 SDS-Page gel of (**A**) Car9 tagged sfGFP in different locations (**B**) and Car9 variant K8AK11A.

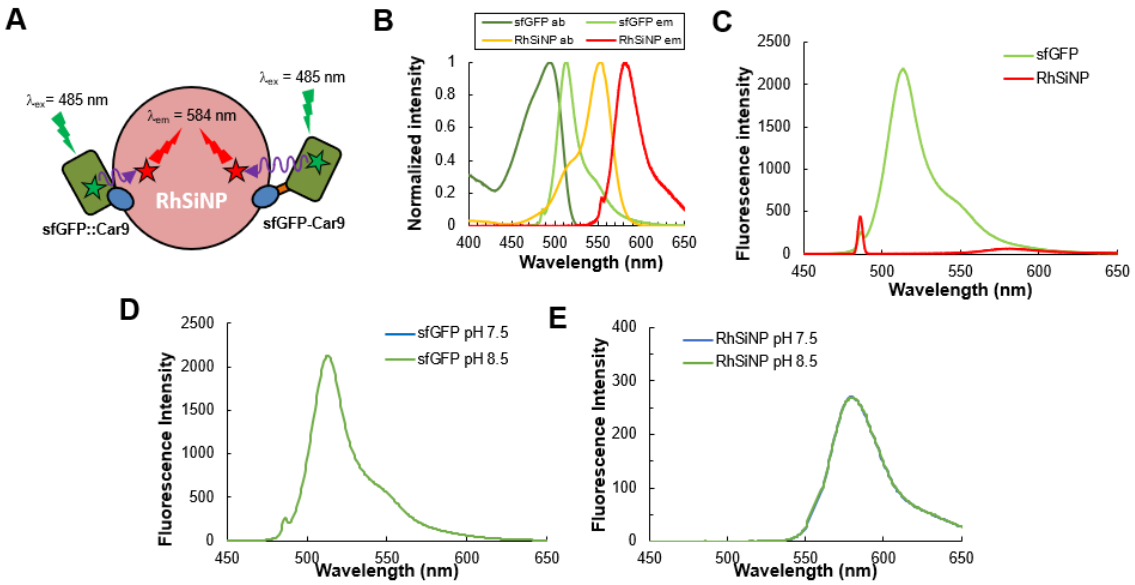

Figure A.2: (A) Schematic representation of the hybrid FRET system. Possible adsorbed poses for sfGFP-Car9 and sfGFP::Car9 are shown to illustrate the different donor-acceptor geometries. The sfGFP chromophore (green star) is situated in the upper third of the b-barrel. Rhodamine acceptors (red stars) are expected to be randomly distributed within silica nanoparticles. (B) Normalized absorption (ab) and emission (em) spectra of sfGFP and 10 nm RhSiNP; sfGFP has a maximum emission peak at 512 nm when excited at 485 nm, while RhSiNP exhibits maximum adsorption at 554 nm and emits at 584 nm. The shaded region corresponds to the overlap between the emission spectrum of sfGFP and the absorption spectrum of RhSiNP. FRET spectra recorded at pH 7.5 (C) Emission spectra of 5µM sfGFP (green) and 1µM RhSiNP (red) upon excitation at λ_{ex}=485 nm (D). Emission spectra of 5µM sfGFP at pH 7.5 (green) and pH 8.5 (blue) upon excitation at λ_{ex}=485 nm. (E) Emission spectra of 1µM RhSiNP at pH 7.5 (green) and pH 8.5 (blue) upon excitation at λ_{ex}=554 nm.

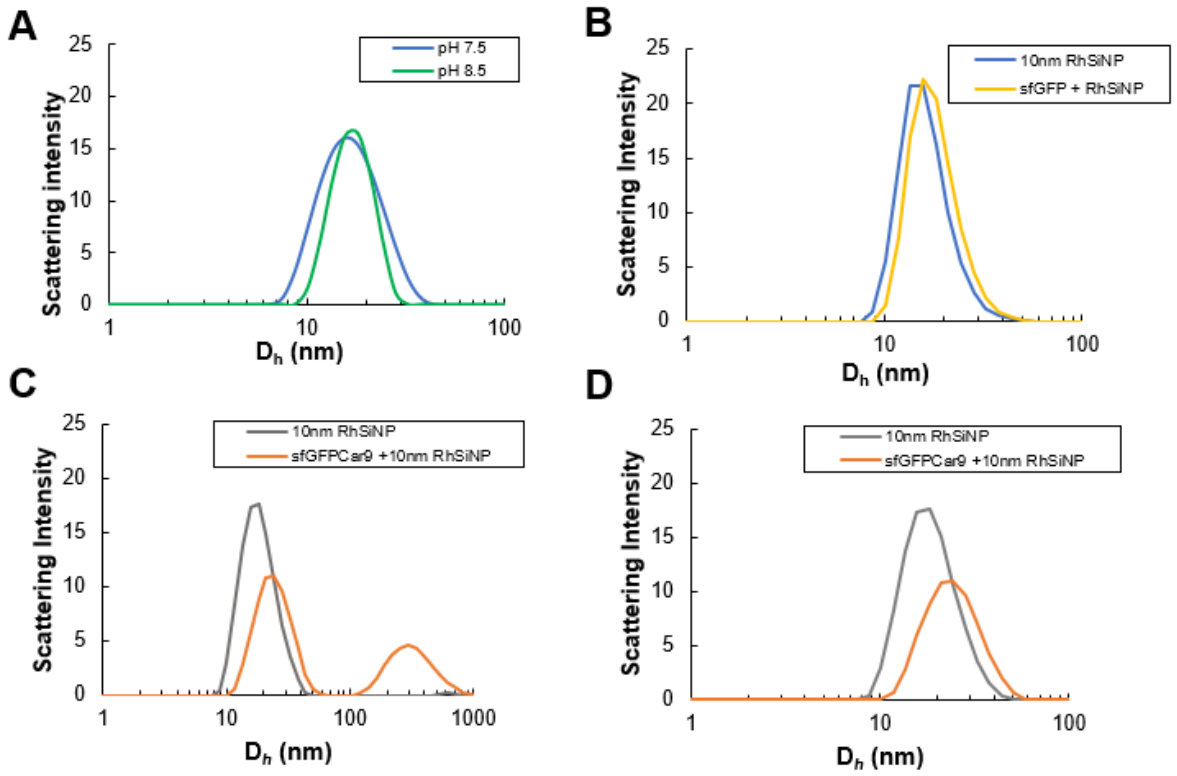

Figure A.3: (**A**)Size distribution of pure 10nm RhSiNP in 20 mM Tris-HCl at pH 7.5 (blue) and 8.5 (green), (**B**) size distribution of pure 10nm RhSiNP (blue) or sfGFP-RhSiNP (yellow) at pH 7.5, (**C**) 10nm RhSiNP (grey) or 10nm RhSiNP and sfGFP-Car9 (orange) at pH 7.5, **(D**)and 10nm RhSiNP (grey) or 10nm RhSiNP and sfGFP::Car9 (orange) in 20mM Tris-HCl, pH 7.5 (data for figure A.2D collected by Yundi Zhao)**.**

Table 2: Zeta Potential (mV) of 10nm RhSiNP and aggregates at different pH (*Data collected by Yundi Zhao)

Sample	10nm NP	
	pH = 7.5	pH = 8.5
sfGFP::Car9-Car9	-7.1 ± 0.5	-9.5 ± 1.3
sfGFP::Car9-K8AK11A	-5.2 ± 0.8	-8.5 ± 2.3
RhSiNP	-24.7 ± 0.5	-34.9 ± 9.9
RhSiNP@sfGFP::Car9-Car9*	-19.8 ± 1.1	-24.8 ± 0.75
RhSiNP@sfGFP::Car9-K8AK11A	-16.6 ± 4.3	-21.3 ± 1.2

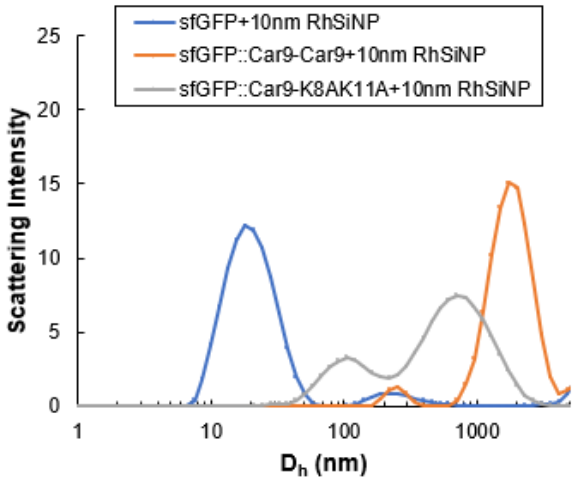

A.4. Low concentration mixture of protein and 10nm RhSiNP showing similar trends to higher concentration mixtures at the same 5:1 ratio.

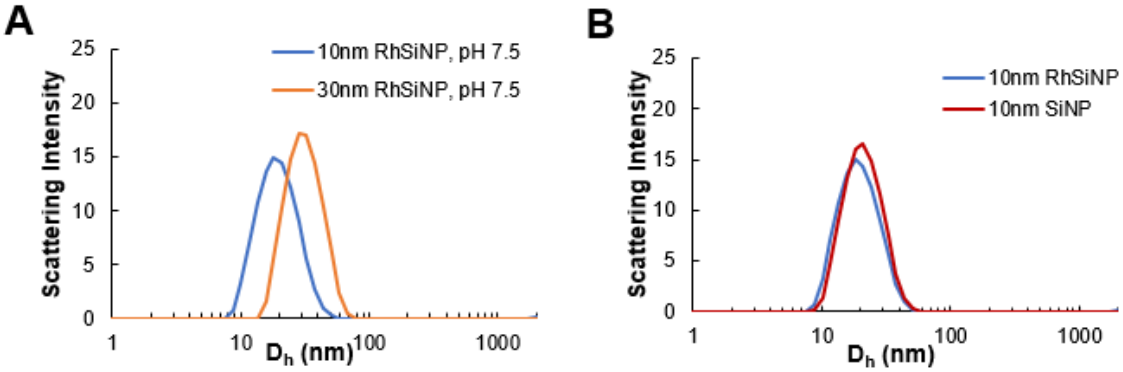

Figure A.5 (**A**)Size distribution of pure 10nm RhSiNP in 20 mM Tris-HCl at pH 7.5 (blue) and 30nm RhSiNP (orange), (**B**) size distribution of pure 10nm RhSiNP (blue) or 10nm SiNP (red) at pH 7.5 in 20mM Tris-HCl.

Table 3: Zeta Potential of 30nm RhSiNP and aggregates at different pH

Sample	30nm RhSiNP		10nm SiNP	
	pH = 7.5	pH = 8.5	pH = 7.5	pH = 8.5
RhSiNP	-22.5 ± 2.3	-38.0 ± 12.8	-13.9 ± 3.2	-15.4± 2.9
RhSiNP@sfGFP::Car9-Car9	-20.2 ± 0.8	-24.1 ± 1.6	-	-
RhSiNP@sfGFP::Car9-K8AK11A	-20.3 ± 0.8	-22.1 ± 0.5	-	-

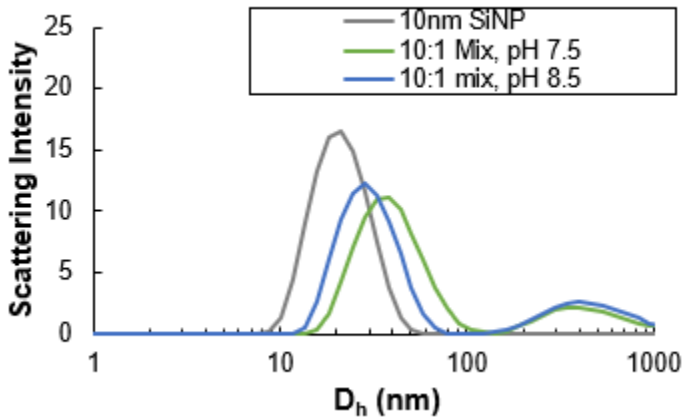

Figure A.6. Size distribution of sfGFP::Car9-K8AK11A with 10nm SiNP.

Appendix B. Supplementary Information for Chapter 3

DNA Sequences used to make each protein from Chapter 3. Capital letters represent the sequence of the expressed protein and the lowercase letter represent the Gibson overlaps as well as any DNA not expressed as a protein.

Ank1C2_1-
gggaattgtgagcggataacaattcccctctagaaataattttgtttaactttaagaaggagatatacatATGGGCTCTTGGGGC
AGCTCTGAACTGGGTAAACGTCTGATCGAAGCGGCTGAAAACGGCAACAAAGACCG
CGTTAAAGATCTGATTGAAAACGGTGCCGACGTGAACGCGTCCGACTCTGATGGTCG
CACCCCGCTTCACCATGCTGCAGAAAACGGCCACGCGGAAGTTGTAGCGCTGCTGA
TCGAAAAAGGTGCAGATGTTAACGCGAAGGACAGCGACGGCCGTACCCCGCTGCAT
CATGCCGCTGAAAACGGCCACGATGAAGTGGTCCTGATCCTTCTGCTGAAAGGTGCG
GACGTGAACGCTAAAGATTCCGACGGCCGCACCCCGCTGCATCACGCTGCGGAAAA
CGGTCACAAACGCGTGGTTCTGGTTCTGATTCTGGCCGGCGCTGACGTGAACACCTC
TGATTCTGATGGTCGTACCCCGCTGGACCTGGCGCGTGAACATGGTAACGAAGAAGT
TGTGAAGGCACTTGAAAAACAGtaataactcgagcaccaccaccaccaccactgagatccg

Ank3C2_1-
gggaattgtgagcggataacaattcccctctagaaataattttgtttaactttaagaaggagatatacatATGTCTGAACTGGGC
AAACGTCTGATCGAAGCAGCGGAAAACGGCAACAAAGACCGTGTGAAAGATCTGCT
CGAAAACGGTGCTGACGTTAACGCCAGCGATTCCGACGGTAAAACCCCGCTGCACC
TGGCAGCCGAAAACGGCCATGCGAAGGTGGTTCTGCTGCTTCTGGAACAGGGTGCT
GACCCGAACGCGAAAGATAGCGATGGCAAAACCCCGCTGCATCTGGCTGCGGAAAA
CGGTCACGCCGTTGTAGTGGCTCTGCTCCTGATGCACGGTGCAGACCCGAACGCCAA
AGACTCCGATGGCAAGACCCCGCTGCATCTGGCGGCAGAAAACGGCCATGAAGAAG
TTGTGATCCTGCTTCTGGCGATGGGCGCTGACCCGAACACCTCTGACTCTGATGGTC
GTACCCCGCTGGATCTGGCGCGTGAACACGGTAACGAAGAAGTCGTTAAAGTCCTG
GAAGATCATGGCGGTTGGCTGGAAtaataactcgagcaccaccaccaccaccactgagatccg

1na0C3_3-
gggaattgtgagcggataacaattcccctctagaaataattttgtttaactttaagaaggagatatacatATGAACCTGGCGGAA
AAAATGTACAAGGCCGGTAACGCGATGTACCGTAAAGGCCAGTACACCATTGCGAT
CATCGCTTACACCCTGGCACTGCTGAAGGATCCGAATAACGCAGAGGCTTGGTATAA
CCTGGGCAACGCGGCGTACAAAAAAGGTGAATACGATGAAGCCATTGAAGCATACC
AGAAAGCGCTTGAACTGGATCCGAACAACGCGGAAGCTTGGTACAATCTGGGTAAC
GCCTACTACAAGCAGGGCGATTACGACGAAGCCATCGAATACTACCAGAAAGCGCT
GGAACTCGACCCGAACAACGCAGAAGCTAAACAGAACCTGGGTAACGCTAAGCAG
AAACAGGGCCTGGAAtaataactcgagcaccaccaccaccaccactgagatccggctgctaacaaagcc

HR00C3_2-
gggaattgtgagcggataacaattcccctctagaaataattttgtttaactttaagaaggagatatacatATGATTGAAGAAGTT
GTTGCTGAAATGATCGATATTCTTGCGGAGTCTTCTAAGAAAAGCATTGAGGAACTG
GCCCGTGCTGCGGACAACAAAACCACTGAAAAAGCTGTTGCGGAAGCCATCGAAGA
GATCGCGCGCCTTGCGACCGCCGCTATTCAGCTGATTGAGGCTCTGGCAAAGAACCT
GGCTTCCGAAGAGTTCATGGCGCGCGCAATCAGCGCGATTGCTGAACTGGCTAAAA
AGGCGATCGAGGCGATCTACCGTCTTGCAGATAATCACACCACTGACACCTTTATGG
CTCGTGCAATTGCCGCGATCGCTAACCTGGCGGTTACCGCTATTCTCGCGATCGCTG
CTCTGGCCTCTAACCATACTACCGAAGAATTCATGGCCCGTGCTATTTCCGCTATCG
CGGAACTTGCTAAAAAGGCAATTGAAGCGATCTACCGCCTGGCTGACAACCATACG
ACTGATAAATTTATGGCCGCTGCTATCGAAGCTATCGCTCTGCTGGCAACCCTGGCC
ATCCTGGCTATTGCGCTTCTGGCCTCCAACCATACTACGGAGGAGTTTATGGCTAAA
GCCATCAGCGCTATCGCTGAGCTGGCCAAAAAGGCTATTGAGGCTATCTACCGTCTG
GCAGACAACCATACCTCTCCGACCTACATCGAAAAGGCTATTGAAGCAATTGAGAA
GATTGCCCGCAAAGCTATCAAGGCCATCGAAATGCTGGCTAAAAACATTACTACTG
AAGAATACAAGGAAAAGGCCAAGAGCGCTATCGACGAAATCCGTGAGAAAGCTAA
GGAAGCCATTAAACGCCTGGAAGATAACCGTACCCTGGAAtaataactcgagcatcaccaccatcat
cactgagatccg

Ank1C4_2-
gggaattgtgagcggataacaattcccctctagaaataattttgtttaactttaagaaggagatatacatATGTCTGAAGATGGT
GAACTGCTGATTCTGGCTGCGGAACTGGGTATTGCAGAAGCTGTACGCATGCTGATC
GAACAGGGCGCCGACGTTAACGCTTCCGACGATGACGGTCGCACTCCGCTTCACCAT
GCTGCGGAAAACGGCCATCTGGCTGTAGTGCTGCTTCTGCTGCTGAAAGGCGCGGAT
GTGAACGCTAAAGATTCTGACGGCCGTACTCCGCTGCATCATGCTGCTGAAAACGGT
CACAAAACCGTTGTTCTGCTTCTTATCCTGATGGGTGCTGATGTTAACGCTAAGGATT
CCGATGGCCGCACCCCGCTTCACCACGCGGCGGAAAACGGTCATAAAGAAGTGGTT
AAACTGCTGATTCGCAAGGGCGCAGACGTTAACACCTCTGACTCGGACGGTCGTACT
CCGCTTGATCTGGCCCGTGAACATGGCAACGAAGAAGTTGTTAAACTGCTGGAAAA
ACAGCTGGAAtaataactcgagcaccaccaccaccaccactgagatccg

Tj10C4_G1-
gggaattgtgagcggataacaattcccctctagaaataattttgtttaactttaagaaggagatatacatATGGACGAATGCGAA
GAAAAAGCTCGCCGTGTGGCGGAAAAAGTGGAACGTCTGAAACGTTCCGGTACCTC
TGAAGACGAAATTGCGGAAGAAGTTGCACGTGAAATCTCCGAAGTTATCCGTACCC
TTAAAGAATCCGGTTCTTCTTACGAAGTCATTTGCGAATGCGTGGCTCGTATTGTTGC
TGAAATCGTGGAGGCACTGAAGCGTTCGGGTACCTCCGCGGTAGAAATTGCAAAAA
TCGTCGCGCGCGTGATCTCTGAAGTTATCCGTACCCTGAAAGAATCTGGTAGCTCTT
ACGAAGTTATTTGCGAATGCGTAGCACGCATCGTTGCTGAAATTGTCGAAGCGCTGA
AACGTTCCGGTACGTCCGCTGCGATCATTGCTCTTATTGTGGCACTGGTTATCTCTGA
AGTGATTCGCACCCTGAAGGAGTCCGGCTCTTCGTCTTTCGAAGTCATCCTTGAATG
CGTGATCCGCATCGTGCTGGAAATTATCGAAGCTCTGAAACGTTCTGGTACCTCTGA
ACAGGACGTTATGCTGATTGTAATGGCGGTGCTTCTGGTTGTTCTGGCGACCCTGCA
GCTGTCTGGTTCTtaataactcgagcaccaccaccaccaccactgagatccg

Car9-Ank1C2_1-
gggaattgtgagcggataacaattcccctctagaaataattttgtttaactttaagaaggagatatacatATGGACAGTGCTCGC
GGGTTTAAAAAGCCTGGGAAGCGGGGCGGCGGCTCTGAAAACTTATACTTTCAGTC
CATGGGGGGCTCTTGGGGCAGCTCTGAACTGGGTAAACGTCTGATCGAAGCGGCTG
AAAACGGCAACAAAGACCGCGTTAAAGATCTGATTGAAAACGGTGCCGACGTGAAC
GCGTCCGACTCTGATGGTCGCACCCCGCTTCACCATGCTGCAGAAAACGGCCACGCG
GAAGTTGTAGCGCTGCTGATCGAAAAAGGTGCAGATGTTAACGCGAAGGACAGCGA
CGGCCGTACCCCGCTGCATCATGCCGCTGAAAACGGCCACGATGAAGTGGTCCTGA
TCCTTCTGCTGAAAGGTGCGGACGTGAACGCTAAAGATTCCGACGGCCGCACCCCG
CTGCATCACGCTGCGGAAAACGGTCACAAACGCGTGGTTCTGGTTCTGATTCTGGCC
GGCGCTGACGTGAACACCTCTGATTCTGATGGTCGTACCCCGCTGGACCTGGCGCGT
GAACATGGTAACGAAGAAGTTGTGAAGGCACTTGAAAAACAG
taataactcgagcaccaccaccaccaccactgagatccg

Ank3C2_1-Car9-
gggaattgtgagcggataacaattcccctctagaaataattttgtttaactttaagaaggagatatacatATGTCTGAACTGGGC
AAACGTCTGATCGAAGCAGCGGAAAACGGCAACAAAGACCGTGTGAAAGATCTGCT
CGAAAACGGTGCTGACGTTAACGCCAGCGATTCCGACGGTAAAACCCCGCTGCACC
TGGCAGCCGAAAACGGCCATGCGAAGGTGGTTCTGCTGCTTCTGGAACAGGGTGCT
GACCCGAACGCGAAAGATAGCGATGGCAAAACCCCGCTGCATCTGGCTGCGGAAAA
CGGTCACGCCGTTGTAGTGGCTCTGCTCCTGATGCACGGTGCAGACCCGAACGCCAA
AGACTCCGATGGCAAGACCCCGCTGCATCTGGCGGCAGAAAACGGCCATGAAGAAG
TTGTGATCCTGCTTCTGGCGATGGGCGCTGACCCGAACACCTCTGACTCTGATGGTC
GTACCCCGCTGGATCTGGCGCGTGAACACGGTAACGAAGAAGTCGTTAAAGTCCTG
GAAGATCATGGCGGTTGGCTGGAAAAGCTTGGCGGCGGCTCTGACAGTGCTCGCGG
GTTTAAAAAGCCTGGGAAGCGGtaataactcgagcaccaccaccaccaccactgagatccg

1na0C3_3-Car9-
gggaattgtgagcggataacaattcccctctagaaataattttgtttaactttaagaaggagatatacatATGAACCTGGCGGAA
AAAATGTACAAGGCCGGTAACGCGATGTACCGTAAAGGCCAGTACACCATTGCGAT
CATCGCTTACACCCTGGCACTGCTGAAGGATCCGAATAACGCAGAGGCTTGGTATAA
CCTGGGCAACGCGGCGTACAAAAAAGGTGAATACGATGAAGCCATTGAAGCATACC
AGAAAGCGCTTGAACTGGATCCGAACAACGCGGAAGCTTGGTACAATCTGGGTAAC
GCCTACTACAAGCAGGGCGATTACGACGAAGCCATCGAATACTACCAGAAAGCGCT
GGAACTCGACCCGAACAACGCAGAAGCTAAACAGAACCTGGGTAACGCTAAGCAG
AAACAGGGCCTGGAAAAGCTTGGCGGCGGCTCTGACAGTGCTCGCGGGTTTAAAAA
GCCTGGGAAGCGGtaataactcgagcaccaccaccaccaccactgagatccggctgctaacaaagcc

HR00C3_2-Car9-
gggaattgtgagcggataacaattcccctctagaaataattttgtttaactttaagaaggagatatacatATGATTGAAGAAGTT
GTTGCTGAAATGATCGATATTCTTGCGGAGTCTTCTAAGAAAAGCATTGAGGAACTG
GCCCGTGCTGCGGACAACAAAACCACTGAAAAAGCTGTTGCGGAAGCCATCGAAGA
GATCGCGCGCCTTGCGACCGCCGCTATTCAGCTGATTGAGGCTCTGGCAAAGAACCT
GGCTTCCGAAGAGTTCATGGCGCGCGCAATCAGCGCGATTGCTGAACTGGCTAAAA
AGGCGATCGAGGCGATCTACCGTCTTGCAGATAATCACACCACTGACACCTTTATGG
CTCGTGCAATTGCCGCGATCGCTAACCTGGCGGTTACCGCTATTCTCGCGATCGCTG
CTCTGGCCTCTAACCATACTACCGAAGAATTCATGGCCCGTGCTATTTCCGCTATCG
CGGAACTTGCTAAAAAGGCAATTGAAGCGATCTACCGCCTGGCTGACAACCATACG
ACTGATAAATTTATGGCCGCTGCTATCGAAGCTATCGCTCTGCTGGCAACCCTGGCC
ATCCTGGCTATTGCGCTTCTGGCCTCCAACCATACTACGGAGGAGTTTATGGCTAAA
GCCATCAGCGCTATCGCTGAGCTGGCCAAAAAGGCTATTGAGGCTATCTACCGTCTG
GCAGACAACCATACCTCTCCGACCTACATCGAAAAGGCTATTGAAGCAATTGAGAA
GATTGCCCGCAAAGCTATCAAGGCCATCGAAATGCTGGCTAAAAACATTACTACTG
AAGAATACAAGGAAAAGGCCAAGAGCGCTATCGACGAAATCCGTGAGAAAGCTAA
GGAAGCCATTAAACGCCTGGAAGATAACCGTACCCTGGAAAAGCTTGGCGGCGGCT
CTGACAGTGCTCGCGGGTTTAAAAAGCCTGGGAAGCGGtaataactcgagcatcaccaccatcatcact
gagatccg

Ank1C4_2-Car9-
gggaattgtgagcggataacaattcccctctagaaataattttgtttaactttaagaaggagatatacatATGTCTGAAGATGGT
GAACTGCTGATTCTGGCTGCGGAACTGGGTATTGCAGAAGCTGTACGCATGCTGATC
GAACAGGGCGCCGACGTTAACGCTTCCGACGATGACGGTCGCACTCCGCTTCACCAT
GCTGCGGAAAACGGCCATCTGGCTGTAGTGCTGCTTCTGCTGCTGAAAGGCGCGGAT
GTGAACGCTAAAGATTCTGACGGCCGTACTCCGCTGCATCATGCTGCTGAAAACGGT
CACAAAACCGTTGTTCTGCTTCTTATCCTGATGGGTGCTGATGTTAACGCTAAGGATT
CCGATGGCCGCACCCCGCTTCACCACGCGGCGGAAAACGGTCATAAAGAAGTGGTT
AAACTGCTGATTCGCAAGGGCGCAGACGTTAACACCTCTGACTCGGACGGTCGTACT
CCGCTTGATCTGGCCCGTGAACATGGCAACGAAGAAGTTGTTAAACTGCTGGAAAA
ACAGCTGGAAAAGCTTGGCGGCGGCTCTGACAGTGCTCGCGGGTTTAAAAAGCCTG
GGAAGCGG taataactcgagcaccaccaccaccaccactgagatccg

Car9-Tj10C4_G1-
gggaattgtgagcggataacaattcccctctagaaataattttgtttaactttaagaaggagatatacatATGGACAGTGCTCGC
GGGTTTAAAAAGCCTGGGAAGCGGGGCGGCGGCTCTGAAAACTTATACTTTCAGTC
CATGGGGGACGAATGCGAAGAAAAAGCTCGCCGTGTGGCGGAAAAAGTGGAACGT
CTGAAACGTTCCGGTACCTCTGAAGACGAAATTGCGGAAGAAGTTGCACGTGAAAT
CTCCGAAGTTATCCGTACCCTTAAAGAATCCGGTTCTTCTTACGAAGTCATTTGCGA
ATGCGTGGCTCGTATTGTTGCTGAAATCGTGGAGGCACTGAAGCGTTCGGGTACCTC
CGCGGTAGAAATTGCAAAAATCGTCGCGCGCGTGATCTCTGAAGTTATCCGTACCCT
GAAAGAATCTGGTAGCTCTTACGAAGTTATTTGCGAATGCGTAGCACGCATCGTTGC
TGAAATTGTCGAAGCGCTGAAACGTTCCGGTACGTCCGCTGCGATCATTGCTCTTAT
TGTGGCACTGGTTATCTCTGAAGTGATTCGCACCCTGAAGGAGTCCGGCTCTTCGTC
TTTCGAAGTCATCCTTGAATGCGTGATCCGCATCGTGCTGGAAATTATCGAAGCTCT
GAAACGTTCTGGTACCTCTGAACAGGACGTTATGCTGATTGTAATGGCGGTGCTTCT
GGTTGTTCTGGCGACCCTGCAGCTGTCTGGTTCTtaataactcgagcaccaccaccaccaccactgagatcc
g

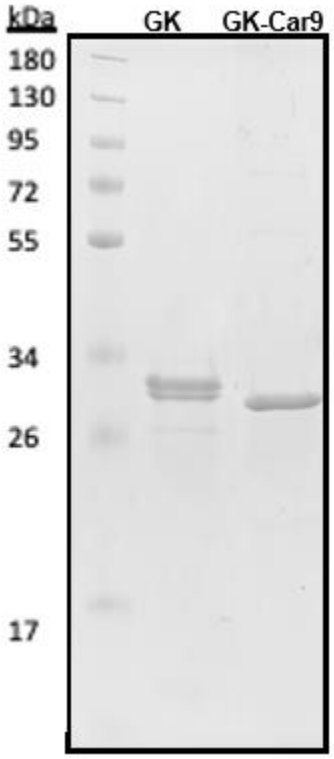

Figure B.1. SDS gel of glucokinase-car9 and glucokinase monomers.

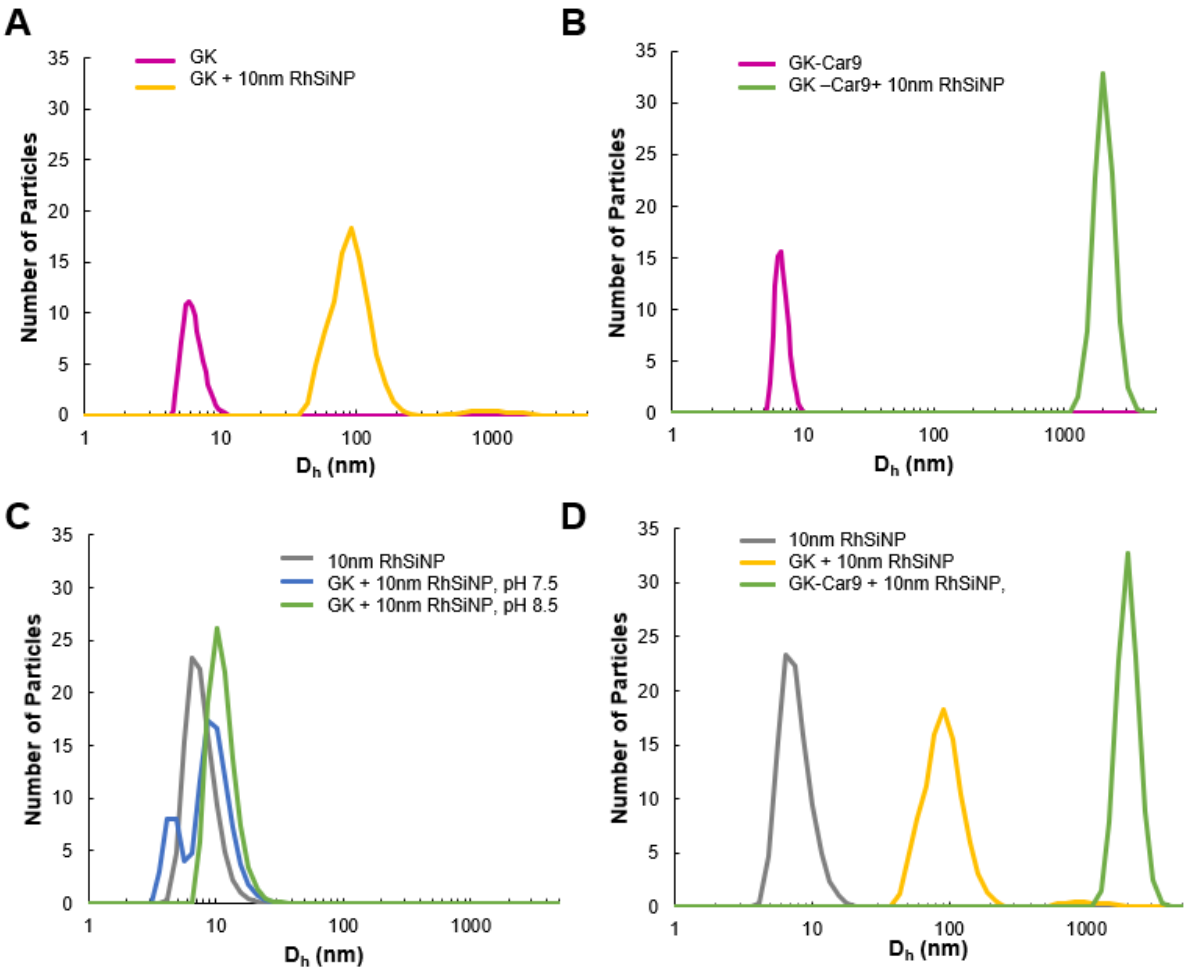

Figure B.2(**A**) Size distribution of 5µM GK (pink) and GK and 10nm RhSiNP system (yellow) with 5 µM GK and 1µM 10nm RhSiNP in 20mM Tris HCl, pH 7.5. (**B**) Size distribution of 5µM GK-Car9 (pink) and GK-Car9 and 10nm RhSiNP system (blue) with 5µM GK-Car9 and 1µM 10nm RhSiNP in 20mM Tris HCl, pH 7.5. (**C**) Size distribution of 1µM 10nm RhSiNP (grey) or GK and 10nm RhSiNP system with 3 µM GK and 1µM 10nm RhSiNP in 20mM Tris HCl, pH 7.5 (blue) and pH 8.5 (green). (**D**) Size distribution of 1µM 10nm RhSiNP (grey) or GK and 10nm RhSiNP system (yellow) with 5 µM GK and 1µM 10nm RhSiNP and the GK-Car9 and 10nm RhSiNP system (blue) with 5µM GK-Car9 and 1µM 10nm RhSiNP in 20mM Tris HCl, pH 7.5. This is a repeat of Figures 3.1 and 3.2 but using the number distribution instead of intensity.

Appendix C. Supplementary Information for Chapter 4

DNA Sequences used to make each ZnS binding protein. Capital letters represent the sequence of the expressed protein and the lowercase letter represent the Gibson overlaps as well as any DNA not expressed as a protein.

sfGFP::CT43

gggaattgtgagcggataacaattcccctctagaaataattttgtttaactttaagaaggagatatacatATGCGTAAAGGCGAA
GAGCTGTTCACTGGTGTCGTCCCTATTCTGGTGGAACTGGATGGTGATGTCAACGGT
CATAAGTTTTCCGTGCGTGGCGAGGGTGAAGGTGACGCAACTAATGGTAAACTGAC
GCTGAAGTTCATCTGTACTACTGGTAAACTGCCGGTACCTTGGCCGACTCTGGTAAC
GACGCTGACTTATGGTGTTCAGTGCTTTGCTCGTTATCCGGACCACATGAAGCAGCA
TGACTTCTTCAAGTCCGCCATGCCGGAAGGCTATGTGCAGGAACGCACGATTTCCTT
TAAGGATGACGGCACGTACAAAACGCGTGCGGAAGTGAAATTTGAAGGCGATACCC
TGGTAAACCGCATTGAGCTGAAAGGCATTGACTTTAAAGAAGACGGCAATATCCTG
GGCCATAAGCTGGAATACAATTTTAACAGCCACAATGTTTACATCACCGCCGATAAA
CAAAAAAATGGCATTAAAGCGAATTTTAAAATTCGCCACAACGTGGAGGGCTCTGC
GGGTGACAGCTCTGGCGTGGATTCCCGTAGCGTTACCTCCGATGGCAGCGTGCAGCT
GGCTGATCACTACCAGCAAAACACTCCAATCGGTGATGGTCCTGTTCTGCTGCCAGA
CAATCACTATCTGAGCACGCAAAGCGTTCTGTCTAAAGATCCGAACGAGAAACGCG
ATCACATGGTTCTGCTGGAGTTCGTAACCGCAGCGGGCATCACGCATGGTATGGATG
AACTGTACAAAtaataactcgagcaccaccaccaccaccactgagatccg

sfGFP::CT43-CT43

gggaattgtgagcggataacaattcccctctagaaataattttgtttaactttaagaaggagatatacatATGCGTAAAGGCGAA
GAGCTGTTCACTGGTGTCGTCCCTATTCTGGTGGAACTGGATGGTGATGTCAACGGT
CATAAGTTTTCCGTGCGTGGCGAGGGTGAAGGTGACGCAACTAATGGTAAACTGAC
GCTGAAGTTCATCTGTACTACTGGTAAACTGCCGGTACCTTGGCCGACTCTGGTAAC
GACGCTGACTTATGGTGTTCAGTGCTTTGCTCGTTATCCGGACCACATGAAGCAGCA
TGACTTCTTCAAGTCCGCCATGCCGGAAGGCTATGTGCAGGAACGCACGATTTCCTT
TAAGGATGACGGCACGTACAAAACGCGTGCGGAAGTGAAATTTGAAGGCGATACCC
TGGTAAACCGCATTGAGCTGAAAGGCATTGACTTTAAAGAAGACGGCAATATCCTG
GGCCATAAGCTGGAATACAATTTTAACAGCCACAATGTTTACATCACCGCCGATAAA
CAAAAAAATGGCATTAAAGCGAATTTTAAAATTCGCCACAACGTGGAGGGCTCTGC
GGGTGACAGCTCTGGCGTTGATTCTCGTAGCGTTACCTCCGATGGCAGCGTGCAGCT
GGCTGATCACTACCAGCAAAACACTCCAATCGGTGATGGTCCTGTTCTGCTGCCAGA
CAATCACTATCTGAGCACGCAAAGCGTTCTGTCTAAAGATCCGAACGAGAAACGCG
ATCACATGGTTCTGCTGGAGTTCGTAACCGCAGCGGGCATCACGCATGGTATGGATG
AACTGTACAAAAAGCTTGGCGGCGGCTCTGCCGGTGATAGCTCCGGCGTGGATTCCC
GTAGCGTGTAAtaataactcgagcaccaccaccaccaccactgagatccg

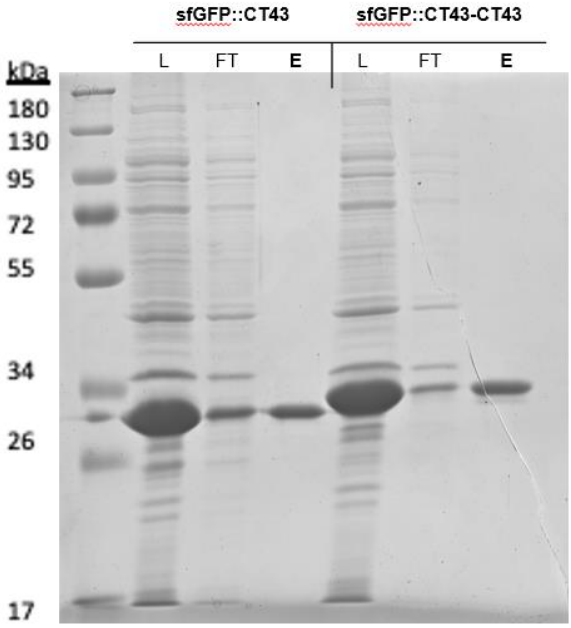

Figure C.1. SDS gel of ZnS binding derivatives of sfGFP. Includes load to column (L), flowthrough (FT), and elution (E).

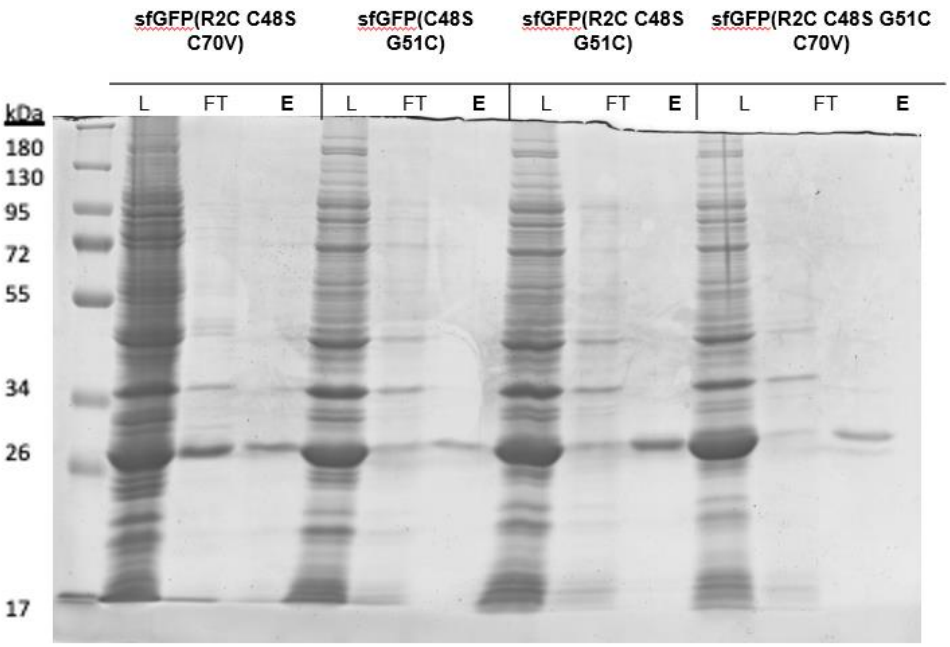

Figure C.2. SDS gel of cysteine mutated sfGFP. Includes load to column (L), flow-through (FT), and elution (E).

References

(1) Dickerson, M. B.; Sandhage, K. H.; Naik, R. R. Protein- and Peptide-Directed Syntheses of Inorganic Materials. *Chem. Rev.* **2008**, *108* (11), 4935–4978. https://doi.org/10.1021/cr8002328.

(2) Sarikaya, M.; Tamerler, C.; Schwartz, D. T.; Baneyx, F. Materials Assembly and Formation Using Engineered Polypeptides. *Annual Review of Materials Research* **2004**, *34* (1), 373–408. https://doi.org/10.1146/annurev.matsci.34.040203.121025.

(3) Sarikaya, M.; Tamerler, C.; Jen, A. K.-Y.; Schulten, K.; Baneyx, F. Molecular Biomimetics: Nanotechnology through Biology. *Nature Mater* **2003**, *2* (9), 577–585. https://doi.org/10.1038/nmat964.

(4) Berg, J. C. *An Introduction to Interfaces & Colloids: The Bridge to Nanoscience*; World Scientific Publishing Co. Pte. Ltd.: Hackensack, N.J., 2010.

(5) Arole, D. V. M.; Munde, P. S. V. FABRICATION OF NANOMATERIALS BY TOP-DOWN AND BOTTOM-UP APPROACHES – AN OVERVIEW; 2014.

(6) Boal, A. K.; Ilhan, F.; DeRouchey, J. E.; Thurn-Albrecht, T.; Russell, T. P.; Rotello, V. M. Self-Assembly of Nanoparticles into Structured Spherical and Network Aggregates. *Nature* **2000**, *404* (6779), 746–748. https://doi.org/10.1038/35008037.

(7) Mendes, A. C.; Baran, E. T.; Reis, R. L.; Azevedo, H. S. Self-Assembly in Nature: Using the Principles of Nature to Create Complex Nanobiomaterials. *Wiley Interdisciplinary Reviews: Nanomedicine and Nanobiotechnology* **2013**, *5* (6), 582–612. https://doi.org/10.1002/wnan.1238.

(8) Baneyx, F.; Schwartz, D. T. Selection and Analysis of Solid-Binding Peptides. *Curr. Opin. Biotechnol.* **2007**, *18* (4), 312–317. https://doi.org/10.1016/j.copbio.2007.04.008.

(9) Dickerson, M. B.; Sandhage, K. H.; Naik, R. R. Protein- and Peptide-Directed Syntheses of Inorganic Materials. *Chem. Rev.* **2008**, *108* (11), 4935–4978. https://doi.org/10.1021/cr8002328.

(10) Saveleva, M. S.; Eftekhari, K.; Abalymov, A.; Douglas, T. E. L.; Volodkin, D.; Parakhonskiy, B. V.; Skirtach, A. G. Hierarchy of Hybrid Materials—The Place of Inorganics-in-Organics in It, Their Composition and Applications. *Front. Chem.* **2019**, *7*. https://doi.org/10.3389/fchem.2019.00179.

(11) Nanomaterials Definition Matters. *Nature Nanotechnology* **2019**, *14* (3), 193–193. https://doi.org/10.1038/s41565-019-0412-3.

(12) Ozin, G. A.; Yang, S. M. The Race for the Photonic Chip: Colloidal Crystal Assembly in Silicon Wafers. *Advanced Functional Materials* **2001**, *11* (2), 95–104. https://doi.org/10.1002/1616-3028(200104)11:2<95::AID-ADFM95>3.0.CO;2-O.

(13) van Blaarderen, A.; Ruel, R.; Wiltzius, P. Template-Directed Colloidal Crystallization. *Nature* **1997**, *385*, 321–324.

(14) Yi, G.-R.; Thorsen, T.; Manoharan, V. N.; Hwang, M.-J.; Jeon, S.-J.; Pine, D. J.; Quake, S. R.; Yang, S.-M. Generation of Uniform Colloidal Assemblies in Soft Microfluidic Devices. *Advanced Materials* **2003**, *15* (15), 1300–1304. https://doi.org/10.1002/adma.200304890.

(15) Plunkett, K. N.; Mohraz, A.; Haasch, R. T.; Lewis, J. A.; Moore, J. S. Light-Regulated Electrostatic Interactions in Colloidal Suspensions. *J. Am. Chem. Soc.* **2005**, *127* (42), 14574–14575. https://doi.org/10.1021/ja054666a.

(16) Ge, J.; Yin, Y. Magnetically Responsive Colloidal Photonic Crystals. *J. Mater. Chem.* **2008**, *18* (42), 5041–5045. https://doi.org/10.1039/B809958H.

(17) Hecht, F. M.; Bausch, A. R. Kinetically Guided Colloidal Structure Formation. *Proc Natl Acad Sci USA* **2016**, *113* (31), 8577–8582. https://doi.org/10.1073/pnas.1605114113.
(18) Macfarlane, R. J.; Lee, B.; Jones, M. R.; Harris, N.; Schatz, G. C.; Mirkin, C. A. Nanoparticle Superlattice Engineering with DNA. *Science* **2011**, *334* (6053), 204–208. https://doi.org/10.1126/science.1210493.
(19) Park, S. Y.; Lytton-Jean, A. K. R.; Lee, B.; Weigand, S.; Schatz, G. C.; Mirkin, C. A. DNA-Programmable Nanoparticle Crystallization. *Nature* **2008**, *451* (7178), 553–556. https://doi.org/10.1038/nature06508.
(20) Mirkin, C. A.; Letsinger, R. L.; Mucic, R. C. A DNA-Based Method for Rationally Assembling Nanoparticles into Macroscopic Materials. 3.
(21) Alivisatos, A. P.; Johnsson, K. P.; Peng, X.; Wilson, T. E.; Loweth, C. J.; Bruchez, M. P.; Schultz, P. G. Organization of "nanocrystal Molecules" Using DNA. *Nature* **1996**, *382* (6592), 609–611. https://doi.org/10.1038/382609a0.
(22) Biancaniello, P. L.; Kim, A. J.; Crocker, J. C. Colloidal Interactions and Self-Assembly Using DNA Hybridization. *Phys. Rev. Lett.* **2005**, *94* (5), 058302. https://doi.org/10.1103/PhysRevLett.94.058302.
(23) De Fazio, A. F.; El-Sagheer, A. H.; Kahn, J. S.; Nandhakumar, I.; Burton, M. R.; Brown, T.; Muskens, O. L.; Gang, O.; Kanaras, A. G. Light-Induced Reversible DNA Ligation of Gold Nanoparticle Superlattices. *ACS Nano* **2019**, *13* (5), 5771–5777. https://doi.org/10.1021/acsnano.9b01294.
(24) Yi, C.; Yang, Y.; Liu, B.; He, J.; Nie, Z. Polymer-Guided Assembly of Inorganic Nanoparticles. *Chem. Soc. Rev.* **2020**, *49* (2), 465–508. https://doi.org/10.1039/C9CS00725C.
(25) Moaseri, E.; Bollinger, J. A.; Changalvaie, B.; Johnson, L.; Schroer, J.; Johnston, K. P.; Truskett, T. M. Reversible Self-Assembly of Glutathione-Coated Gold Nanoparticle Clusters via PH-Tunable Interactions. *Langmuir* **2017**, *33* (43), 12244–12253. https://doi.org/10.1021/acs.langmuir.7b02446.
(26) Sohn, B. H.; Seo, B. H. Fabrication of the Multilayered Nanostructure of Alternating Polymers and Gold Nanoparticles with Thin Films of Self-Assembling Diblock Copolymers. *Chem. Mater.* **2001**, *13* (5), 1752–1757. https://doi.org/10.1021/cm000939j.
(27) Lin, Y.; Daga, V. K.; Anderson, E. R.; Gido, S. P.; Watkins, J. J. Nanoparticle-Driven Assembly of Block Copolymers: A Simple Route to Ordered Hybrid Materials. *J. Am. Chem. Soc.* **2011**, *133* (17), 6513–6516. https://doi.org/10.1021/ja2003632.
(28) Tsutsumi, K.; Funaki, Y.; Hirokawa, Y.; Hashimoto, T. Selective Incorporation of Palladium Nanoparticles into Microphase-Separated Domains of Poly(2-Vinylpyridine)-Block-Polyisoprene. *Langmuir* **1999**, *15* (16), 5200–5203. https://doi.org/10.1021/la990246l.
(29) Taladriz-Blanco, P.; Buurma, N. J.; Rodríguez-Lorenzo, L.; Pérez-Juste, J.; Liz-Marzán, L. M.; Hervés, P. Reversible Assembly of Metal Nanoparticles Induced by Penicillamine. Dynamic Formation of SERS Hot Spots. *J. Mater. Chem.* **2011**, *21* (42), 16880–16887. https://doi.org/10.1039/C1JM12175H.
(30) Cheng, L.; Liu, A.; Peng, S.; Duan, H. Responsive Plasmonic Assemblies of Amphiphilic Nanocrystals at Oil−Water Interfaces. *ACS Nano* **2010**, *4* (10), 6098–6104. https://doi.org/10.1021/nn101685q.

(31) Li, F.; Josephson, D. P.; Stein, A. Colloidal Assembly: The Road from Particles to Colloidal Molecules and Crystals. *Angew. Chem. Int. Ed. Engl.* **2011**, *50* (2), 360–388. https://doi.org/10.1002/anie.201001451.
(32) Zhao, Y.; Thorkelsson, K.; Mastroianni, A. J.; Schilling, T.; Luther, J. M.; Rancatore, B. J.; Matsunaga, K.; Jinnai, H.; Wu, Y.; Poulsen, D.; Fréchet, J. M. J.; Paul Alivisatos, A.; Xu, T. Small-Molecule-Directed Nanoparticle Assembly towards Stimuli-Responsive Nanocomposites. *Nature Materials* **2009**, *8* (12), 979–985. https://doi.org/10.1038/nmat2565.
(33) Dhami, N. K.; Reddy, M. S.; Mukherjee, A. Biomineralization of Calcium Carbonates and Their Engineered Applications: A Review. *Front. Microbiol.* **2013**, *4*. https://doi.org/10.3389/fmicb.2013.00314.
(34) Nakamura, Y.; Mochida, A.; Choyke, P. L.; Kobayashi, H. Nanodrug Delivery: Is the Enhanced Permeability and Retention Effect Sufficient for Curing Cancer? *Bioconjugate Chem.* **2016**, *27* (10), 2225–2238. https://doi.org/10.1021/acs.bioconjchem.6b00437.
(35) Swift, B. J. F.; Shadish, J. A.; DeForest, C. A.; Baneyx, F. Streamlined Synthesis and Assembly of a Hybrid Sensing Architecture with Solid Binding Proteins and Click Chemistry. *J. Am. Chem. Soc.* **2017**, *139* (11), 3958–3961. https://doi.org/10.1021/jacs.7b00519.
(36) Raucher, D.; Chilkoti, A. Enhanced Uptake of a Thermally Responsive Polypeptide by Tumor Cells in Response to Its Hyperthermia-Mediated Phase Transition. *Cancer Res* **2001**, *61* (19), 7163–7170.
(37) Dominguez-Medina, S.; Kisley, L.; Tauzin, L. J.; Hoggard, A.; Shuang, B.; D. S. Indrasekara, A. S.; Chen, S.; Wang, L.-Y.; Derry, P. J.; Liopo, A.; Zubarev, E. R.; Landes, C. F.; Link, S. Adsorption and Unfolding of a Single Protein Triggers Nanoparticle Aggregation. *ACS Nano* **2016**, *10* (2), 2103–2112. https://doi.org/10.1021/acsnano.5b06439.
(38) Zhang, D.; Neumann, O.; Wang, H.; Yuwono, V. M.; Barhoumi, A.; Perham, M.; Hartgerink, J. D.; Wittung-Stafshede, P.; Halas, N. J. Gold Nanoparticles Can Induce the Formation of Protein-Based Aggregates at Physiological PH. *Nano Lett.* **2009**, *9* (2), 666–671. https://doi.org/10.1021/nl803054h.
(39) Bharti, B.; Meissner, J.; Findenegg, G. H. Aggregation of Silica Nanoparticles Directed by Adsorption of Lysozyme. *Langmuir* **2011**, *27* (16), 9823–9833. https://doi.org/10.1021/la201898v.
(40) Care, A.; Bergquist, P. L.; Sunna, A. Solid-Binding Peptides: Smart Tools for Nanobiotechnology. *Trends in Biotechnology* **2015**, *33* (5), 259–268. https://doi.org/10.1016/j.tibtech.2015.02.005.
(41) Coyle, B. L.; Rolandi, M.; Baneyx, F. Carbon-Binding Designer Proteins That Discriminate between Sp2- and Sp3-Hybridized Carbon Surfaces. *Langmuir* **2013**, *29*, 4839–4846.
(42) Patwardhan, S. V.; Emami, F. S.; Berry, R. J.; Jones, S. E.; Naik, Rajesh. R.; Deschaume, O.; Heinz, H.; Perry, C. C. Chemistry of Aqueous Silica Nanoparticle Surfaces and the Mechanism of Selective Peptide Adsorption. *J. Am. Chem. Soc.* **2012**, *134* (14), 6244–6256. https://doi.org/10.1021/ja211307u.
(43) Coyle, B. L.; Baneyx, F. A Cleavable Silica-Binding Affinity Tag for Rapid and Inexpensive Protein Purification. *Biotechnology and Bioengineering* **2014**, *111* (10), 2019–2026. https://doi.org/10.1002/bit.25257.

(44) Dunakey, S. J. G.; Coyle, B. L.; Thomas, A.; Xu, M.; Swift, B. J. F.; Baneyx, F. Selective Labeling and Decoration of the Ends and Sidewalls of Single-Walled Carbon Nanotubes Using Mono- and Bispecific Solid-Binding Fluorescent Proteins. *Bioconjug. Chem.* **2019**, *30* (3), 959–965. https://doi.org/10.1021/acs.bioconjchem.9b00097.
(45) Coyle, B. L.; Baneyx, F. Direct and Reversible Immobilization and Microcontact Printing of Functional Proteins on Glass Using a Genetically Appended Silica-Binding Tag. *Chem. Commun.* **2016**, *52* (43), 7001–7004. https://doi.org/10.1039/C6CC02660E.
(46) Soto-Rodríguez, J.; Coyle, B. L.; Samuelson, A.; Aravagiri, K.; Baneyx, F. Affinity Purification of Car9-Tagged Proteins on Silica Matrices: Optimization of a Rapid and Inexpensive Protein Purification Technology. *Protein Expression and Purification* **2017**, *135*, 70–77. https://doi.org/10.1016/j.pep.2017.05.003.
(47) Yang, W.; Hellner, B.; Baneyx, F. Self-Immobilization of Car9 Fusion Proteins within High Surface Area Silica Sol-Gels and Dynamic Control of Protein Release. *Bioconjug. Chem.* **2016**, *27* (10), 2450–2459. https://doi.org/10.1021/acs.bioconjchem.6b00406.
(48) Hellner, B.; Lee, S. B.; Subramaniam, A.; Subramanian, V. R.; Baneyx, F. Modeling the Cooperative Adsorption of Solid-Binding Proteins on Silica: Molecular Insights from Surface Plasmon Resonance Measurements. *Langmuir* **2019**, *35* (14), 5013–5020. https://doi.org/10.1021/acs.langmuir.9b00283.
(49) Hellner, B.; Alamdari, S.; Pyles, H.; Zhang, S.; Prakash, A.; Sprenger, K. G.; De Yoreo, J. J.; Baker, D.; Pfaendtner, J.; Baneyx, F. Sequence–Structure–Binding Relationships Reveal Adhesion Behavior of the Car9 Solid-Binding Peptide: An Integrated Experimental and Simulation Study. *J. Am. Chem. Soc.* **2020**, *142* (5), 2355–2363. https://doi.org/10.1021/jacs.9b11617.
(50) Parida, S. K.; Dash, S.; Patel, S.; Mishra, B. K. Adsorption of Organic Molecules on Silica Surface. *Advances in Colloid and Interface Science* **2006**, *121* (1), 77–110. https://doi.org/10.1016/j.cis.2006.05.028.
(51) Puddu, V.; Perry, C. C. Interactions at the Silica–Peptide Interface: The Influence of Particle Size and Surface Functionality. *Langmuir* **2014**, *30* (1), 227–233. https://doi.org/10.1021/la403242f.
(52) Lowe, B. M.; Skylaris, C.-K.; Green, N. G. Acid-Base Dissociation Mechanisms and Energetics at the Silica–Water Interface: An Activationless Process. *Journal of Colloid and Interface Science* **2015**, *451*, 231–244. https://doi.org/10.1016/j.jcis.2015.01.094.
(53) Boese, J. N.; Zhao, Y.; Hellner, B. *Submitted* **2020**.
(54) Hench, L. L. Bioceramics: From Concept to Clinic. *J American Ceramic Society* **1991**, *74* (7), 1487–1510. https://doi.org/10.1111/j.1151-2916.1991.tb07132.x.
(55) Kresge, C. T.; Leonowicz, M. E.; Roth, W. J.; Vartuli, J. C.; Beck, J. S. Ordered Mesoporous Molecular Sieves Synthesized by a Liquid-Crystal Template Mechanism. *Nature* **1992**, *359* (6397), 710–712. https://doi.org/10.1038/359710a0.
(56) Wang, M.; Marepally, S. K.; Vemula, P. K.; Xu, C. Chapter 5 - Inorganic Nanoparticles for Transdermal Drug Delivery and Topical Application. In *Nanoscience in Dermatology*; Hamblin, M. R., Avci, P., Prow, T. W., Eds.; Academic Press: Boston, 2016; pp 57–72. https://doi.org/10.1016/B978-0-12-802926-8.00005-7.
(57) Verwey, E. J. W. Theory of the Stability of Lyophobic Colloids. *J. Phys. Chem.* **1947**, *51* (3), 631–636. https://doi.org/10.1021/j150453a001.

(58) Parida, S. K.; Dash, S.; Patel, S.; Mishra, B. K. Adsorption of Organic Molecules on Silica Surface. *Adv Colloid Interface Sci* **2006**, *121* (1–3), 77–110. https://doi.org/10.1016/j.cis.2006.05.028.
(59) Kobayashi, M.; Juillerat, F.; Galletto, P.; Bowen, P.; Borkovec, M. Aggregation and Charging of Colloidal Silica Particles: Effect of Particle Size. *Langmuir* **2005**, *21* (13), 5761–5769. https://doi.org/10.1021/la046829z.
(60) Wu, X.; Narsimhan, G. Effect of Surface Concentration on Secondary and Tertiary Conformational Changes of Lysozyme Adsorbed on Silica Nanoparticles. *Biochimica et Biophysica Acta (BBA) - Proteins and Proteomics* **2008**, *1784* (11), 1694–1701. https://doi.org/10.1016/j.bbapap.2008.06.008.
(61) Puddu, V.; Perry, C. C. Peptide Adsorption on Silica Nanoparticles: Evidence of Hydrophobic Interactions. *ACS Nano* **2012**, *6* (7), 6356–6363. https://doi.org/10.1021/nn301866q.
(62) Förster, T. Zwischenmolekulare Energiewanderung und Fluoreszenz. *Annalen der Physik* **1948**, *437* (1–2), 55–75. https://doi.org/10.1002/andp.19484370105.
(63) Piston, D. W.; Kremers, G.-J. Fluorescent Protein FRET: The Good, the Bad and the Ugly. *Trends Biochem. Sci.* **2007**, *32* (9), 407–414. https://doi.org/10.1016/j.tibs.2007.08.003.
(64) *Handbook of Biological Confocal Microscopy*, 3rd ed.; Pawley, J., Ed.; Springer US, 2006. https://doi.org/10.1007/978-0-387-45524-2.
(65) Lunz, M.; Bradley, A. L.; Gerard, V. A.; Byrne, S. J.; Gun'ko, Y. K.; Lesnyak, V.; Gaponik, N. Concentration Dependence of Forster Resonant Energy Transfer between Donor and Acceptor Nanocrystal Quantum Dot Layers: Effect of Donor-Donor Interactions. *Phys. Rev. B* **2011**, *83* (11), 115423. https://doi.org/10.1103/PhysRevB.83.115423.
(66) Fábián, Á. I.; Rente, T.; Szöllősi, J.; Mátyus, L.; Jenei, A. Strength in Numbers: Effects of Acceptor Abundance on FRET Efficiency. *ChemPhysChem* **2010**, *11* (17), 3713–3721. https://doi.org/10.1002/cphc.201000568.
(67) Abedi, M. R.; Caponigro, G.; Kamb, A. Green Fluorescent Protein as a Scaffold for Intracellular Presentation of Peptides. *Nucleic Acids Res* **1998**, *26* (2), 623–630.
(68) Kim, K.-M.; Kim, H. M.; Lee, W.-J.; Lee, C.-W.; Kim, T.; Lee, J.-K.; Jeong, J.; Paek, S.-M.; Oh, J.-M. Surface Treatment of Silica Nanoparticles for Stable and Charge-Controlled Colloidal Silica. *Int J Nanomedicine* **2014**, *9* (Suppl 2), 29–40. https://doi.org/10.2147/IJN.S57922.
(69) Sikora, A.; Shard, A. G.; Minelli, C. Size and ζ-Potential Measurement of Silica Nanoparticles in Serum Using Tunable Resistive Pulse Sensing. *Langmuir* **2016**, *32* (9), 2216–2224. https://doi.org/10.1021/acs.langmuir.5b04160.
(70) Bhattacharjee, S. DLS and Zeta Potential – What They Are and What They Are Not? *Journal of Controlled Release* **2016**, *235*, 337–351. https://doi.org/10.1016/j.jconrel.2016.06.017.
(71) February 1, P.; Share, 2013. An Overview of the Zeta Potential - Part 1: The Concept http://www.americanpharmaceuticalreview.com/Featured-Articles/133232-An-Overview-of-the-Zeta-Potential-Part-1-The-Concept/ (accessed Mar 29, 2020).
(72) Macfarlane, R. J.; Lee, B.; Jones, M. R.; Harris, N.; Schatz, G. C.; Mirkin, C. A. Nanoparticle Superlattice Engineering with DNA. *Science* **2011**, *334* (6053), 204–208. https://doi.org/10.1126/science.1210493.

(73) Fallas, J. A.; Ueda, G.; Sheffler, W.; Nguyen, V.; McNamara, D. E.; Sankaran, B.; Pereira, J. H.; Parmeggiani, F.; Brunette, T. J.; Cascio, D.; Yeates, T. R.; Zwart, P.; Baker, D. Computational Design of Self-Assembling Cyclic Protein Homo-Oligomers. *Nature Chem* **2017**, *9* (4), 353–360. https://doi.org/10.1038/nchem.2673.
(74) Tomita, K.; Nagata, K.; Kondo, H.; Shiraishi, T.; Tsubota, H.; Suzuki, H.; Ochi, H. Thermostable Glucokinase from Bacillus Stearothermophilus and Its Analytical Application. *Annals of the New York Academy of Sciences* **1990**, *613* (1), 421–425. https://doi.org/10.1111/j.1749-6632.1990.tb18191.x.
(75) Cossairt, B. M. Shining Light on Indium Phosphide Quantum Dots: Understanding the Interplay among Precursor Conversion, Nucleation, and Growth. *Chem. Mater.* **2016**, *28* (20), 7181–7189. https://doi.org/10.1021/acs.chemmater.6b03408.
(76) Suzuki, T.; Arai, S.; Takeuchi, M.; Sakurai, C.; Ebana, H.; Higashi, T.; Hashimoto, H.; Hatsuzawa, K.; Wada, I. Development of Cysteine-Free Fluorescent Proteins for the Oxidative Environment. *PLoS One* **2012**, *7* (5). https://doi.org/10.1371/journal.pone.0037551.
(77) Aldaye, F. A.; Palmer, A. L.; Sleiman, H. F. Assembling Materials with DNA as the Guide. *Science* **2008**, *321* (5897), 1795–1799. https://doi.org/10.1126/science.1154533.